Control of vertebrate core PCP protein localization and dynamics by Prickle2

Mitchell T. Butler[1] and John B. Wallingford[1,2*]

[1]Department of Molecular Biosciences

[2]Howard Hughes Medical Institute

University of Texas at Austin

*To whom correspondence should be addressed:

University of Texas, Dept. of Molecular Biosciences

Patterson Labs

2401 Speedway

Austin, Tx. 78712

512-232-2784

Wallingford@austin.utexas.edu

Keywords: Planar Cell Polarity, Core PCP, Prickle, Pk2, Dishevelled, Dvl1, Van Gogh-like, Vangl1, cilia, multiciliated cell, *Xenopus*

Development ● Accepted manuscript

© 2015. Published by The Company of Biologists Ltd.

Development ● Accepted manuscript

Summary

Planar cell polarity (PCP) is a ubiquitous property of animal tissues and is essential for morphogenesis and homeostasis. In most cases, this fundamental property is governed by a deeply conserved set of "Core PCP" proteins, which includes the transmembrane proteins Van Gogh-like (Vangl) and Frizzled (Fzd), as well as the cytoplasmic effectors Prickle (Pk) and Dishevelled (Dvl). Asymmetric localization of these proteins is thought to be central to their function, and understanding the dynamics of these proteins is an important challenge in developmental biology. Among the processes that are organized by the core PCP proteins is the directional beating of cilia, such as those in vertebrate node, airway and brain. Here, we exploit the live imaging capabilities of *Xenopus* to chart the progressive asymmetric localization of fluorescent reporters of Dvl1, Pk2 and Vangl1 in a planar polarized ciliated epithelium. Using this system, we also characterize the influence of Pk2 on asymmetric dynamics of Vangl1 at the cell cortex, and we define regions of Pk2 that control its own localization and those impacting Vangl1. Finally, our data reveal a striking uncoupling of Vangl1 and Dvl1 asymmetry. This study advances our understanding of conserved PCP protein functions and also establishes a rapid, tractable platform to facilitate future *in vivo* studies of vertebrate PCP protein dynamics.

Introduction

The polarization of cellular shape, structure and behavior across epithelial sheets is established by the action of the Planar Cell Polarity (PCP) pathway. Pioneering work in *Drosophila* revealed that the coordinated orientation of bristles and hairs throughout the body is governed by the "core PCP" genes (Adler, 1992; Gubb, 1993; Gubb and Garcia-Bellido, 1982), and this genetic module has been associated with a diverse set of developmental processes since, spanning from invertebrates to mammals. Some examples in vertebrates include polarized cell shape changes and rearrangements during gastrulation, axis elongation and neural tube closure, the polarized orientation of nodal cilia required during establishment of left-right asymmetry, polarized beating of cilia on multiciliated cells, and the polarization of cochlear mechanosensory stereocilia (Goodrich and Strutt, 2011; Gray et al., 2011; Wallingford, 2012).

A hallmark of planar polarized epithelia is the asymmetric localization of core PCP proteins in each cell. The core PCP genes include the transmembrane proteins Frizzled (Fz), Van Gogh (Vang or Strabismus [Stbm] in invertebrates, Vangl in vertebrates), and Flamingo (Fmi or Starry night [Stan] in invertebrates, Celsr in vertebrates), as well as intracellular proteins Dishevelled (Dsh, Dvl in vertebrates), Diego (Dgo, inversin in vertebrates), and Prickle (Pk) (Strutt, 2008). These proteins form complementary domains of enrichment at the level of apical junctions within the cells comprising planar-polarized epithelia. In the *Drosophila* wing, for example, the localization of Fz and Dsh becomes restricted to the distal edge of the apical cell membrane, and these PCP complexes are mirrored at the proximal edge by accumulations of Vang and Pk (Axelrod, 2001; Bastock et al., 2003; Strutt, 2001; Strutt and Strutt, 2002). Both proximal and distal complexes associate with Fmi, and together, they pattern the orientation of wing hairs from levels of high Fz in one cell towards low levels of Fz across shared junctions in the neighboring cells (Adler et al., 1997; Chen et al., 2008; Strutt and Strutt, 2008). The transmembrane proteins are sufficient to propagate PCP patterning signals between cells in a non-autonomous fashion, coordinating alignment, while the cytoplasmic members amplify intracellular asymmetry (Adler et al., 2000; Das et al., 2004; Jenny et al., 2003; Jenny et al., 2005; Strutt and Strutt, 2007; Strutt and Strutt, 2008; Tree et al., 2002; Vinson and Adler, 2002; Wu and Mlodzik, 2008).

In the fly wing, core PCP proteins are initially trafficked apically and are symmetrically distributed at the level of cellular junctions. Transmembrane Fmi is thought to be subject to endocytic flux, and stability at the membrane is gradually increased over time in a Fz- and Vang-dependent manner, presumably as these core PCP complexes become associated with Fmi/Vang or Fmi/Fz pairs of a neighboring cell (Strutt et al., 2011). The preferential stabilization of Fmi-Vangl pairs at proximal junctions and Fmi-Fz pairs at distal junctions has been suggested to involve an initial upstream bias that is then amplified via both positive and negative feedback loops (Amonlirdviman et al., 2005; Tree et al., 2002). These proposed feedback loops that amplify intracellular PCP asymmetry have been shown in *Drosophila* to involve a network of positive and negative interactions centered on the cytoplasmic core PCP members (Cho et al., 2015; Strutt and Strutt, 2007). In brief, Pk binds and inhibits membrane localization of Dsh, but Dgo competes with Pk for Dsh binding, promoting the association of Dsh with Fz (Jenny et al., 2005; Tree et al., 2002). Pk also physically interacts with Vang, and this interaction leads to the clustering of Vang on the opposite side of the cell (Bastock et al., 2003; Jenny et al., 2003; Strutt et al., 2011). In addition, Pk mediates the internalization

Development • Accepted manuscript

of Vang or Fmi/Vang molecules that are not associated with stable, patterned complexes (Cho et al., 2015). Because of the delicate balance required for asymmetry between these proteins, an intricate system of ubiquitination and proteosomal degradation is in place to control the protein levels of core PCP components (Cho et al., 2015; Narimatsu et al., 2009; Strutt et al., 2013a; Strutt et al., 2013b), and overexpression or loss of function of one core PCP protein in a given cell is generally sufficient to disrupt core PCP asymmetry and consequently result in a loss or reversal of structural polarity (Adler et al., 2000; Bastock et al., 2003; Strutt and Strutt, 2007; Tree et al., 2002).

Consistent with data from *Drosophila*, asymmetry has also been observed for various core PCP proteins in multiciliated cells (MCCs) of the mouse airway and brain ventricles (Guirao et al., 2010; Vladar et al., 2012), where these cells drive directional fluid flow that is essential for proper development and homeostasis (Brooks and Wallingford, 2014). Here, PCP proteins control the coordinated orientation of ciliary structures that interface with the apical cytoskeleton within each cell, thus aligning the cilia within these cells to establish polarized, synchronous beating; the term rotational polarity refers to these intracellular orientations of ciliary basal bodies (Wallingford, 2010). Furthermore, the asymmetric patterning of core PCP proteins allows for the alignment of cellular polarity between cells across entire tissues, and this intercellular tissue-wide polarity promotes strong, effective flow (Wallingford, 2010).

In vertebrates, core PCP proteins are encoded by families of related genes, including two Vangl genes and three each of Dvl and Pk genes. Several examples of cell- and tissue-specific differences in protein localization and function have been observed for different vertebrate PCP family members in the context of these multiciliated epithelia. For example, Dvl2 is present at the basal bodies of MCCs, but does not display cortical asymmetry, while Dvl1 and Dvl3 are not at basal bodies, but rather are present at planar-polarized cortical crescents (Park et al., 2008; Vladar et al., 2012). Additional examples of differences in the activity of related core PCP homologs is provided by the analysis of ciliary and cytoskeletal patterning throughout the multicilated ependymal cells of various PCP mutant mice. The ciliary rotational polarity within cells appears to be disrupted in *Celsr2* and *Celsr3* mutants, while the tissue-wide coordination of mean directionality remains intact (Boutin et al., 2014). In stark contrast, *Celsr1* mutant mice exhibit the seemingly opposite characteristics, with properly organized ciliary patches within cells that fail to oriented in a coordinated fashion across cells throughout the tissue (Boutin et al., 2014). The increased complexity seen in

Development ● Accepted manuscript

vertebrate PCP warrants further study of individual core PCP family members and challenging any assumed redundancy in their activity.

Interestingly, MCCs are also present in the epidermis of developing amphibian embryos, and the relative ease of observing these epidermal MCCs has contributed to them being an excellent platform for analysis of planar polarization for decades (König and Hausen, 1993; Twitty, 1928). Early studies of the role for PCP signaling in MCC directional beating were performed in these cells, prefiguring the work in mammals (Mitchell et al., 2009; Park et al., 2008). In this context, disruption of core PCP can lead to defects in either rotational polarity within the cells or tissue-wide polarity across the cells in the *Xenopus* epidermis (Mitchell et al., 2009; Park et al., 2008). For example, the transplantation of epidermal tissue overexpressing Vangl2 onto an otherwise normal embryo reverses the orientation of basal bodies in cells situated anterior to the transplant, demonstrating the tissue-level, non-autonomous effects of transmembrane core PCP components. (Mitchell et al., 2009). In contrast, the expression of a PCP-specific, dominant negative form of Dvl that lacks a large C-terminal portion of the PDZ domain (Dvl2-ΔPDZ$_{partial}$ - previously referred to as Xdd1 (Sokol, 1996)) completely randomizes the initial rotational polarity within MCCs, and tissue-grafting experiments revealed that this Dvl2-ΔPDZ$_{partial}$ dominant negative acts in a strictly cell-autonomous manner (Mitchell et al., 2009). In addition to the basal body localization that was also later reported in the mouse ependyma and MTECs, Dvl2 immunostaining shows symmetrical distributions at the apical junctions of cells regardless of its polarizing effects (Park et al., 2008). In fact, despite the promising capability of dynamic protein studies in this *in vivo* vertebrate system, there is as yet no report of planar-polarized, apicolateral localization of core PCP proteins in the *Xenopus* epidermis. Here, we report that planar polarity of the *Xenopus* mulitciliated epithelium is progressively patterned by the asymmetric localization of a subset of core PCP family members, and we go on to leverage the strengths of this *Xenopus* platform by performing quantitative analyses of subcellular dynamics that serve to dissect the role of Pk2 in the establishment of these asymmetric patterns.

Development ● Accepted manuscript

Development ● Accepted manuscript

Results

Asymmetric patterning of specific core PCP protein family members in *Xenopus* multiciliated cells:

A role for PCP proteins in the orientation of ciliary beating was first described in *Xenopus* epidermal MCCs (Mitchell et al., 2009; Park et al., 2008). Surprisingly, there are as yet no reports of asymmetric localization of PCP proteins at the cell cortex in these cells, though such localization has been reported for both airway and ependymal MCCs in the mouse (Guirao et al., 2010; Vladar et al., 2012). Because vertebrate PCP proteins are encoded by multi-gene families, we surveyed the localization of a wide range of GFP fusions to *Xenopus* PCP proteins, using mosaic expression for accurate assessment of asymmetric localization. While many previously studied *Xenopus* core PCP proteins localized symmetrically around the cell cortex, including Dvl2, Dvl3, Fzd7, Fzd8, and Vangl2, we found that Dvl1, Pk2, Vangl1, and Fzd6, displayed striking asymmetric localizations (Fig. 1 and Fig. S1). Transcripts for eight of these nine family members were identified in RNAseq analyses of organotyic cultures of the *Xenopus* mucociliary epidermis, with only Fzd7 being absent (Chung et al., 2014). In *Xenopus* embryos, fluid flow is directed across the epidermis from the dorsoanterior to ventroposterior direction (Fig. 1A). Accordingly, we observed punctate accumulations of Dvl1-GFP that were restricted to the dorsoanterior apical cell cortex of MCCs found here, corresponding to asymmetry in the direction upstream of flow (Fig. 1B). Mucociliary epithelia are comprised of two principal cell types, MCCs and mucus-secreting goblet cells, and because the MCCs are separated from one another by intervening goblet cells, PCP signaling must be transmitted evenly across both cell types. It is notable then, that we also observed asymmetric accumulations of Dvl1 in goblet cells (Fig. 1C). Comparable asymmetry appeared to occur in other intercalating cell types, such as ioncytes (Dubaissi and Papalopulu, 2011; Quigley et al., 2011) and small secretory cells (Dubaissi et al., 2014; Walentek et al., 2014), which were identifiable by their significantly smaller surface area and lack of cilia in regions where only intercalating cells had been labeled.

Typically, asymmetric Dvl co-accumulates with asymmetric Frizzled at the cell cortex (Seifert and Mlodzik, 2007), and indeed, Fzd6-GFP also localized to the dorsoanterior cell cortex (Fig. S1A). In most planar polarized tissues, domains enriched for Dvl and Fzd are mirrored by complementary accumulations of Prickle and Vangl (Seifert and Mlodzik, 2007), and we observed asymmetric accumulations of GFP-Pk2 (Fig. 1D,E) and GFP-Vangl1 (Fig.

1F,G) at the ventroposterior cell cortex in both MCCs and goblet cells as well. Moreover, co-expression of Dvl1-GFP and RFP-Pk2 revealed mutually exclusive domains of enrichment (Fig. 1H), and clear colocalization was observed for RFP-Pk2 and GFP-Vangl1 proteins (Fig. 1I). These observations of a Fzd family member on the anterior cell face and Vangl at the posterior are consistent with previous functional studies of domineering non-autonomy of PCP signaling in this tissue (Mitchell et al., 2009), though on the other hand, it was surprising that their orientation relative to the direction of ciliary beating is reversed compared to that of MCCs in the mouse trachea (Vladar et al., 2012).

Dynamics of asymmetric localization of Pk2, Vang1 and Dvl1:

Having identified useful reporters for PCP patterning in the *Xenopus* embryonic epidermis, we next sought to characterize the developmental dynamics of core PCP protein localization here. MCCs are derived from a basal layer of progenitor cells and insert into the mucociliary epithelium at the early tailbud stage (~St. 22), after which cilia are assembled and polarization of ciliary beating is established progressively over the next several hours (until roughly St. 30) (Billett and Gould, 1971; Drysdale and Elinson, 1992; König and Hausen, 1993). Prior to the insertion of MCCs, Dvl1-GFP decorated the apicolateral regions of goblet cells symmetrically and in a punctate fashion (Fig. 1J). During tailbud stages, as ciliogenesis is completed and the refinement of ciliary orientation begins, Dvl1-GFP asymmetry is present, though the degree and coordination of asymmetry is variable at this time. Dvl1-GFP asymmetry finally reaches a maximal level in both goblet cells and MCCs across the tissue around stage 30 (Fig. 1K), a time at which ciliary basal body orientations are locked in place and flow has strengthened across the epithelium (König and Hausen, 1993; Mitchell et al., 2007; Werner et al., 2007). GFP-Pk2 displayed similar dynamics to Dvl1-GFP, with asymmetric accumulations also apparent by stage 24-25 that reach a maximum around stage 30 (Fig. 1L,M), though with some notable differences. First, although GFP-Pk2 also localizes symmetrically to apical accumulations just prior to ciliogenesis, the punctate pattern observed for Dvl1-GFP was less prominent for GFP-Pk2 (Fig. 1L). Another interesting dissimilarity was the localization of GFP-Pk2 near ciliary basal bodies labeled with Centrin-RFP at later stages (Fig. S1G). For the transmembrane protein Vangl1, localization of GFP fusions at early stages consisted primarily of cytoplasmic puncta, and labeling at the cell cortex was weak and diffuse at these stages (Fig. 1N). This pattern may reflect the vesicular transport proteins known to be important for the processing and trafficking of Vangl proteins (Guo et al., 2013; Merte et al., 2009; Yin et al., 2012). Both the cortical localization and

Development ● Accepted manuscript

asymmetry of these accumulations increased as development proceeded, with a timeframe similar to that for Dvl1 and Pk2 (Fig. 1O).

We quantified these dynamic localization patterns using the relative level of reporter fluorescence intensity at dorsoanterior and ventroposterior cell cortices, and mosaic labeling allowed us score cells abutting unlabeled neighbors ("PCP Enrichment," see Fig. S5A and Methods). This metric demonstrates the degree to which asymmetry increased over time during PCP patterning for all three reporters examined (Fig. 1P-R). Interestingly, PCP enrichment increased along with increased coordination of fluid flow (König and Hausen, 1993), and asymmetries were not easily detectable at times corresponding to stages of initial MCC intercalations. Once MCCs have intercalated and expanded their apical surface, basal bodies are docked and serve as the foundations for cilia formation. Once these cilia are visibly projecting from the apical surface, the surrounding goblet cells can be seen exhibiting asymmetric patterns that are readily detectible by eye; though no such patterns are easily discernible in the MCCs. This result suggests that the initial rotational polarity of basal bodies that is in place at the onset of ciliogenesis, which clearly depends upon intact Dvl2 function (Mitchell et al., 2007), may not be reliant upon intracellular PCP asymmetry, but rather directional information is imparted by the surrounding tissue. However, it has also been reported that polarity information can be relayed in the absence of detectible asymmetry in the fly wing (Strutt and Strutt, 2007), so perhaps asymmetric stability or activity in the absence of clear asymmetric localization may be present in these early, maturing MCCs.

Interplay of cortical asymmetric localization of Pk2 and Dvl1:

We next explored the interplay among Pk2 and Dvl1 during asymmetric localization, as antagonistic interactions between proteins homologous to them are fundamental to amplifying visual intracellular asymmetry in other contexts (Strutt and Strutt, 2007), yet have never been examined for these particular family members or in this tissue. We first determined the effect of the well-characterized and PCP-specific dominant negative, Dvl2-$\Delta PDZ_{partial}$ (Xdd1) (Sokol, 1996), shown to negatively affect PCP signaling in a variety of contexts, including in MCCs (Park et al., 2008; Wallingford et al., 2000). Expression of Dvl2-$\Delta PDZ_{partial}$ significantly disrupted the normal ventroposterior restriction of Pk2-GFP (Fig. 2A-C), demonstrating asymmetric Pk2 localization is dependent upon the ability of the cell to adopt a planar-polarized state. We then performed the complementary experiment by reducing Pk2 levels using an antisense morpholino (Pk2-MO1) that disrupts splicing of Pk2

Development ● Accepted manuscript

(Fig. S2A). While discrete crescents of Dvl1-GFP accumulation were normally oriented in the dorsoanterior direction in controls (Fig. 2D), Pk2 knockdown significantly reduced this asymmetric enrichment (Fig. 2E,F), and a second morpholino targeting an alternate splicing sequence provided similar results (Fig. S2A-C). Together with the observed progressive asymmetric localization (Fig. 1), these data demonstrate the efficacy and veracity of our GFP reporters for core PCP protein localization in this tissue. We then used these novel reporters to address outstanding questions in vertebrate PCP signaling.

The role of the 'PCP effectors' Intu and Fritz/Wdpcp on Pk2 protein localization:

First, we assessed the role of the "PCP Effector" proteins in the patterning of polarity complexes, as the role for these proteins in PCP signaling remain contentious. First identified as planar polarity proteins by genetic screens in *Drosophila* (Collier et al., 2005; Gubb and Garcia-Bellido, 1982), Inturned and Fritz were placed genetically downstream of core PCP protein function (Collier et al., 2005; Lee and Adler, 2002; Wong and Adler, 1993), though a recent paper suggests that Fritz overexpression can influence core PCP protein localization in *Drosophila* (Wang et al., 2014). Curiously, the vertebrate orthologues, (called Intu and Wdpcp/Fritz) were found to control ciliogenesis, first in the *Xenopus* epidermis (Kim et al., 2010; Park et al., 2006) and later in mice (Cui et al., 2013; Zeng et al., 2010). Intu apparently plays only a modest role in PCP mediated processes such as convergent extension (Park et al., 2006), while Wdpcp is essential for both convergent extension in *Xenopus* (Kim et al., 2010) and planar polarization of cochlear hair cells in the mouse (Cui et al., 2013). We performed knockdown of Wdpcp and Intu using morpholinos whose action has been validated by genetic studies in mice (Cui et al., 2013; Kim et al., 2010; Park et al., 2006; Zeng et al., 2010). Wdpcp knockdown strongly disrupted the planar polarized localization of Pk2, while Intu knockdown had a far more modest, though still significant effect (Fig. 3A-C). These data reveal an important role for Wdpcp in control of core PCP protein asymmetry in vertebrates, the mechanism of which will be important to determine.

Role of Pk2 in the control of asymmetric cortical Vangl1 dynamics

The next question we chose to address concerns the interplay between Pk2 and Vangl1. In *Drosophila*, Pk physically interacts with and clusters Vang at the apicolateral membrane, and this behavior promotes Vang accumulation on the proximal side of cells in the wing epithelium (Bastock et al., 2003; Jenny et al., 2003). Though Vangl2 and Pk1 are implicated in vertebrate PCP (Liu et al., 2014; Song et al., 2010; Takeuchi et al., 2003; Torban et al.,

Development • Accepted manuscript

2008; Vladar et al., 2012), Vangl1 and Pk2 remain relatively seldom studied, and it is unknown in vertebrates if either Pk protein is required for normal localization of either Vangl protein. We found that Pk2 knockdown eliminated the asymmetric accumulation of GFP-Vangl1 at the ventroposterior cell cortex (Fig. 4A,B), while conversely, Pk2 overexpression increased Vangl1 apicolateral enrichment to such a degree that accumulations were no longer as restricted to just ventroposterior regions but rather enriched in other areas around the cell periphery (Fig. 4A,C). Additional analysis confirms that Pk2 knockdown disrupts asymmetry by suppressing the enrichment of Vang1 at the cortical regions of the cell (Fig. S3B), and together, these observations are consistent with a previously defined role for Pk in the clustering of Vang (Bastock et al., 2003; Cho et al., 2015; Strutt and Strutt, 2007). We conclude that Pk2 promotes cortical Vang1 concentration, while an excess of Pk2 promotes further GFP-Vangll enrichment that becomes increasingly unrestricted from the ventroposterior cell face. In the reciprocal experiment, overexpression of Vangl1 showed a clear reduction in the planar-polarized, cortical accumulation of GFP-Pk2 (Fig. S4A-C), while enrichments of Dvl1-GFP were still present yet not asymmetrically polarized (Fig. S4A-C). In light of previous evidence that Vang participates in the control of Pk protein levels (Strutt et al., 2013b), our results suggest that Vangl1 overexpression may be leading to increased levels of Pk2 degradation, which in turn leads to a reduction in Pk2 and associated Dvl1 patterning defects.

Given the demonstrated effects of Pk2 on the asymmetric enrichment of Vangl1, we next asked if Pk2 influences the dynamics of Vangl1 turnover at the cell cortex. Indeed, asymmetric enrichment of Fzd is driven in part by differences in Fzd turnover at distinct locations along the cell cortex (Strutt et al., 2011), and we wanted to test if a similar mechanism may act on Vangl. We therefore measured fluorescence recovery after photobleaching (FRAP) of GFP-Vangl1. In control embryos, enriched regions at the ventroposterior cortex contained a significantly larger stable fraction of GFP-Vangl1 when compared to the less-enriched dorsoanterior cortex (Fig. 4E and Fig. S5C,D). This result was evident as the ~30% increase in normalized fluorescence recovery at the latter (Fig. 4E). This difference was potently extinguished by Pk2 knockdown, in which case both dorsoanterior and ventroposterior cortical regions contain similarly unstable fractions of GFP-Vangl1 (Fig. 4E). In the complementary experiment, overexpression of Pk2 had the opposite effect, eliciting increased stability of GFP-Vangl1 on both sides of the cell (Fig. 4E). Comparison of these measurements to the maximum intensities prior to bleaching (Fig. 4F)

Development ● Accepted manuscript

reveals that areas more highly enriched for GFP-Vangl1 were indeed less dynamic. These data complement the previous work with Dvl-dependent Fzd stabilization in *Drosophila* (Strutt et al., 2011), not only by extending the work to a vertebrate epithelium, but also by demonstrating that asymmetric protein turnover is an attribute of core PCP protein localization on the Vangl/Pk side of the cell.

Structure/function analysis of Pk2:

As the role for Pk2 in the control of core PCP dynamics became quite clear, we sought to determine the structural components of the protein necessary for eliciting the observed polarized behaviors. Pk2 contains three protein domains that are conserved in vertebrate Prickle protein family members and in Prickle proteins across species (Fig. 5A). These include the PET and LIM domains, as well as the C2 domain, which populated by many serines and basic amino acids near the C-terminus of the protein (Jenny et al., 2003; Tree et al., 2002). The roles for various domains of vertebrate Prickle proteins in PCP-dependent processes have been assessed (Daulat et al., 2011; Jenny et al., 2003; Lin and Gubb, 2009; Takeuchi et al., 2003), but how these roles relate to PCP protein localization remains unknown in vertebrates. We therefore constructed three Pk2 deletion constructs corresponding to previously-described versions of *Xenopus* Pk1 (Takeuchi et al., 2003) and *Drosophila* Pk (Jenny et al., 2003); we then assessed both their localizations and their effects of the localization of Vangl1 and Dvll.

We first examined GFP fusions to a deletion of the PET domain and a combined deletion lacking both the PET and LIM domains. Strikingly, both Pk2-ΔPETΔLIM and GFP-Pk2-ΔPET were enriched ventroposteriorly (Fig. 5B,C). While this polarization for GFP-Pk2-ΔPET was not as robust as full-length GFP-Pk2 (Fig. 5E), it was remarkably similar and suggests that neither the PET nor LIM domain is strictly required for proper Pk2 asymmetric localization. Despite their similar localizations, however, these two constructs had divergent effects on Vangl1 when expressed at high levels. Pk2-ΔPETΔLIM severely perturbed not only the asymmetry of Vangl1, but also its association with the cell cortex (Fig. 5F), comparable to the effects of Pk2 knockdown (Fig. S3C). In contrast, both cortical recruitment and asymmetry of Vangl1 were intact after overexpression of Pk2-ΔPET (Fig. 5G) despite a significant reduction in the overall enrichment measure. Together, these findings are consistent with the opposing effects of ΔPETΔLIM and ΔPET deletions of Pk1 on PCP-dependent convergent extension (Takeuchi et al., 2003).

Development • Accepted manuscript

We next assessed a deletion of the C2 domain, which in *Drosophila* allows for binding to Vang, to other Pk molecules, and to Dgo (Jenny et al., 2003). Unlike the other deletions, GFP-Pk2-ΔC2 failed to adopt a polarized localization and instead remained symmetrical around the cell cortex (Fig. 5D,E). As such, this domain appears to be the most essential for normal asymmetric localization of Pk2. Increased expression of Pk2-ΔC2 also severely disrupted the asymmetry of cortical Vangl1, though Vangl1 was present around the cell cortex (Fig. 5H). These data suggest that the C2 domain is required for the regulation of Pk2 localization and that the mislocalization that results from the C2 domain deletion promotes the co-mislocalization of associated Vangl1 (Fig. 5I), though we cannot rule out possibility of an indirect or alternate mechanism of Vangl1 mislocalization around the cortex. Lastly, we used our Pk2 deletions to determine their effects on Dvl1 localization. In *Drosophila*, overexpression of solely the PET and LIM domains together has been suggested to inhibit the membrane association of Dsh (Tree et al., 2002), and the C2 domain that binds Dgo is likely important in the competition between Dgo and Pk for Dsh binding (Jenny et al., 2005). Strikingly, we found that Dvl1 remained polarized in the presence of any of the three Pk2 deletion constructs (Fig. 5J-M), though the degree of was modestly reduced in some cases.

Effects of PCP manipulation on ciliary polarity:

To determine how the various PCP patterning defects we observed affect structural and thus functional polarity in this epithelium, we assessed ciliary orientation using a CLAMP-GFP ciliary rootlet marker and Centrin4-RFP basal body marker (Park et al., 2008). Under control conditions, CLAMP-GFP localized to the dorsoanterior side of basal bodies with little variance, as expected due to striated rootlets being oriented opposite the direction of the effective stroke (Fig. 6A). As previously used to provide ciliary orientation data (Mitchell et al., 2009), we present the state of basal body polarity by using a single arrow for each individual cell in a circular diagram; the points in the mean direction of the effective ciliary strokes, and the length of the arrow represents the mean resultant vector, a measure of variation from the mean orientation within that cell. The majority of cells under control conditions were oriented in the ventroposterior direction, with little variation in the individual orientations observed (Fig. 6B). With an obvious exception for Pk2-ΔPET overexpression, all manipulations that were used to assess the molecular interactions affecting PCP protein enrichment resulted in clear defects in ciliary orientation (Fig. 6C-J). The exception for Pk2-ΔPET overexpression is significant because this reagent also did not disrupt the asymmetry of

Development ● Accepted manuscript

other core PCP proteins (Fig. 5), though this result is dissimilar from a previous report of Pk2-ΔPET overexpression disrupting fly wing hair polarity (Lin and Gubb, 2009). In addition, because Dvl1 and Dvl2 displayed divergent localizations at the cell cortex and basal bodies respectively, we tested the effects of overexpressing Dvl1-$\Delta PDZ_{partial}$, a Dvl1 construct analogous to the Xdd1 deletion of Dvl2 (Mitchell et al., 2009; Park et al., 2008; Sokol, 1996); Similarly to Dvl2-$\Delta PDZ_{partial}$, this resulted in a strong perturbation of ciliary polarity (Fig. 6K,L).

Comparing the mean vector length of individual cells between Pk2 misexpression conditions with that of Vangl1 overexpression reveals a difference in type of polarity defects observed, with seemingly more defective rotational polarity for the former and tissue-wide polarity for the latter. This interpretation is further supported not only by previous characterization of Vangl2 in this respect (Mitchell et al., 2009), but also by a closer examination of Vangl1 overexpression edge of clones, where basal bodies tend to orient their striated rootlets towards higher Vangl1 levels irrespective of their orientation relative to the body axis (Fig. S4B). As would be expected from the observed defects in ciliary orientation upon disrupting core PCP patterning, the resulting strength and directionality of flow at the surface of the embryo was severely impaired upon Pk2 morpholino knockdown and Vangl1 overxpression (Fig. 6N-Q, Supplementary Movie 1-3).

Development ● Accepted manuscript

Discussion

Understanding the dynamics of PCP patterning events *in vivo* provides potential insights regarding the function and interactions of the molecular players involved, yet studies in vertebrates have been limited in this respect. We describe here the action of useful reporters for *in vivo* imaging of the dynamic localization of vertebrate core PCP proteins in *Xenopus*, further supplementing this established rapid and tractable vertebrate PCP model. The observed behavior of symmetrically distributed PCP complexes later resolving into asymmetric accumulations here is reminiscent of early PCP patterning events in the fly wing (Seifert and Mlodzik, 2007; Strutt and Strutt, 2009; Strutt et al., 2011). In addition, there appears to be a common theme of increasing asymmetry coinciding with increasing polarized cellular behaviors. Here, core PCP asymmetry reflects oriented cilia beating, and in

Drosophila wings, the degree of aligned asymmetry of core PCP complexes increasing following hinge contraction and reaches a maximum level just prior to trichome formation (Aigouy et al., 2010; Wong and Adler, 1993). Despite this and other behavioral similarities, these reporters also highlight important differences between planar-polarized tissues and proteins encoded by distinct members of PCP gene families. For example, we previously reported that Dvl2 localizes to basal bodies in MCCs (Park et al., 2008), and here we find Dvl1 localizes to asymmetric cortical crescents, a situation similar to that reported in the mouse airway (Vladar et al., 2012). Similarly, we find that while Vangl2 is cortically localized in this tissue it remains symmetrical; Vangl1 on the other hand becomes progressively planar polarized.

A second notable finding in this respect concerns the relationship between PCP protein asymmetry and the direction of ciliary beating. We find that Pk2/Vangl1 complexes are enriched on the "downstream" side of the cell and thus aligned in the direction of the effective stroke, which is consistent with previous functional studies suggesting that Frizzled points "upstream" of flow (Mitchell et al., 2009). This situation is exactly the opposite of that found in MCCs of the mammalian airway and ependyma, where Prickle and/or Vangl mark the "upstream" face of the cell (Guirao et al., 2010; Vladar et al., 2012). This result argues against there being an intrinsic link between cortical enrichment of core PCP protein complexes and basal body orientation. This notion is consistent with the decoupling of Pk2 localization and kinocilia positioning in the mammalian inner ear (Deans et al., 2007), but it is nonetheless curious in light of the known localization of core PCP proteins to basal bodies (Park et al., 2008; Vladar et al., 2012) and the requirement of intact PCP signaling for asymmetry of the MCC microtubule cytoskeleton (Vladar et al., 2012).

Another related observation of note is the basal body localization of Pk2 we found that was not shown in the murine airway (Vladar et al., 2012). The potential limitations of using synthetic GFP protein fusions necessary for live imaging and the chance of mislocalization should not be ignored, though our particular finding that GFP-Pk2 localizes to basal bodies several stages after ciliogensis is supported by Prickle3 being identified as asymmetrically associating with the more "mature" mother centrioles (but not daughter centrioles) during cell divisions in U-2 OS cells, as well as with the axoneme-associated mother centriole in ciliated hTERT-RPE1 cells (Jakobsen et al., 2011). Determining if Pk2 localization near basal bodies marks or mediates a state in which ciliary orientations are "locked" in place could potentially provide even further insight into the function of this protein in planar polarization.

Development ● Accepted manuscript

How the core planar polarity module interfaces with proteins such as Inturned and Fritz/Wdpcp in vertebrates remains an important question. These proteins have been described as "PCP Effectors" in the fly wing yet have a wide range from strong to mild to no PCP phenotypes in vertebrates depending on the protein in question and the developmental context (Cui et al., 2013; Gray et al., 2009; Kim et al., 2010; Park et al., 2006; Zeng et al., 2010). Further complicating matters is a recent report of both *frtz* overexpression and *fz*/*intu* co-overexpression can effect the patterning of core PCP patterns (Wang et al., 2014), which have been considered to be upstream based on epistasis experiments (Wong and Adler, 1993) and other genetic studies (Collier et al., 2005; Lee and Adler, 2002). However, Intu overexpression alone did not give a significant phenotype in this study (Wang et al., 2014), consistent with previous data showing normal Fz localization in *intu* mutants (Strutt, 2001), mild convergent extension phenotype upon morpholino knockdown in Xenopus gastrulating mesoderm (Park et al., 2006), and only modest PCP pattering effect we see here upon Intu-MO treatment. By contrast, Wdpcp knockdown severely inhibits PCP-dependent convergent extension in *Xenopus* (Kim 2010; Shindo 2014), consistent with the robust effect on the polarized localization of Pk2 here. These data argue that this protein may function independently of Inturned in the control of PCP. Intriguingly, loss of Wdpcp in mice is associated with loss of cortical Vangl2 (Cui et al., 2013).

Additionally, our data shed new light on how mechanisms and relationships identified in *Drosophila* translate to vertebrate PCP signaling, specifically in a multiciliated epithelia consisting of a multi-layered, hetergenous populations of cells shaped by families of PCP proteins acting at multiple levels. In particular, we expand upon relationships established between Vang and Pk (Bastock et al., 2003) and localization dynamics of Fz dependent up Dsh (Strutt et al., 2011) to verify that Pk has an analogous affect on Vangl localization dynamics. Beyond this, we demonstrate the activity of the Pk2 LIM domain is likely to be important for this Vangl-enriching behavior, and we also identify the C2 region as critical for asymmetric cortical localization of Pk2 itself. The fact Dvl1 remained asymmetric under conditions when Vangl1 asymmetry was lost is of particular interest due to scenarios where one core PCP protein is visually asymmetric while others are not being extremely rare, a finding which potentially could be attributed to the increased complexity of vertebrate PCP and lack of similar analysis in vertebrate tissues in general. However, data from *Drosophila* cells argue polarization can occur though Stan/Celsr and Frizzled even in the absence of Vang and obvious asymmetric enrichments (Struhl et al., 2012; Strutt and Strutt, 2007). The

Development ● Accepted manuscript

normal localization of Dvl1 in the face of mislocalized Vangl1 and/or Pk2 could in part be explained by communication from neighboring cells not expressing Pk2 deletions in our mosaic embryos, which would provide further support for Fz/Dsh being the more "dominant" module in comparison to Vangl/Pk (Struhl et al., 2012; Strutt and Strutt, 2007). In addition to providing localization-altering behaviors in the context of previously reported dominant negative activity (Takeuchi et al., 2003), our results provide a cell biological context for previous biochemical data indicating that PET domain function is regulated via intramolecular physical interactions with the LIM domains (Sweede et al., 2008). Ultimately, this work provides a foundation for future studies into the role of vertebrate Prickle proteins, and thus may help to elucidate the etiology of Prickle-associated human pathologies, such as epilepsy, congenital birth defects, and possibly autism (Okumura et al., 2014; Sowers et al., 2013; Tao et al., 2011; Wen et al., 2010).

Development ● Accepted manuscript

MATERIALS AND METHODS

Plasmid and morpholino design

We designed the splice-blocking Pk2 morpholino oligonucleotide based on the longest mRNA seqeuence obtained from the UTexas Oktoberfest gene models available from Xenbase.org. The chosen splice-blocking Pk2-MO#1: GATTGGACAAAGGATTCTCACCTCA is complementary to the region spanning the 3' end of exon 4 and 5' end of intron 4 of sequence JGIv6.000014371_26644_262472 and was prepared by GeneTools, LLC. The second splicing morpholino Pk2-MO#2 has the sequence GAACCCAAACAAACACTTACCTGTT and is complementary to the region spanning the 3' end of exon 3 and 5' end of intron 3.

The Pk2 Primers used for cloning this CDS into Pk2 CS107-GFP using StuI and NotI were:

5'-ATAGGCCTATGTTTAACCGGAGCTCTTGGACAAGGGCTTC -3'
5'-ATGCGGCCGCCTAGGAGATGATGCAATTTTTGCTTTTTCGCCTTT -3'

The remaining gene sequences were cloned into Gateway entry vectors using the Invitrogen pENTR™/D-TOPO® cloning system for recombination of coding sequences into pCSDest GFP or RFP vectors. The sequences and primers used are as follows:

Pk2 for RFP-Pk2

5’-CACCATGTTTAACCGGAGCTCTTGGACAAGGGCTTCCAGC -3’

5’-CTAGGAGATGATGCAATTTTTGCTTTTTCGCCTTTTTCTG -3’

Dvl1 Sequence Genbank BC074103.1 and Primers:

5’-CACCATGGCTGAGACCAAAATCATCTACCATATAGATGAA -3’

5’-CATGATGTCAACAAAGAATTCACAAGGGTTCCCCA -3’

Dvl3 Sequence NCBI ref NM_001092629.1 and Primers:

5’-CACCATGGGGGAGACCAAGGTCATCTACCACCTGGATGAA-3’

5’-AACACCCCAGAATTCTTTGATAACATCCACAAAGAACTCA-3’

Fzd6 Sequence JGIv7b.000063404_134470-165935+ and Primers:

5’-CACCATGGATCTGATTGGCTGCTGCCTCCAAGCTCCGAGC-3’

5’-TCACGCACTTGTCGTATTAATATTAATGTCATTGGCATGG-3’

Vangl1 Sequence JGIv7b.000169011_589431-599179+ and Primers:

5’-CACCATGGACACGGAATCCAACCACTCGGGATATTCACAT-3’

5’-TCACAGGTTGGTCTCAGGTTTGCTACTCACAATGAGACGA-3’

Pk2 Deletions were amplified by fusing 2 PCR products generated with the above and following primers:

ΔPET-1

5’-AGATGGCACCAGTCATGGTTACTGGGAAAAAGTCAAACATCAGCTTGTTC-3’

ΔPET-2

5’-AACTATGAACAAGCTGATGTTTGACTTTTTCCCAGTAACCATGACTGGTG-3’

ΔPETΔLIM-1

5’-AGGCGGAATCTGAAGAGTCCGAGCCATTAAAGTCAAACATCAGCTTGTTC-3’

ΔPETΔLIM-2

5’-AACTATGAACAAGCTGATGTTTGACTTTAATGGCTCGGACTCTTCAGATT-3’

ΔC2-1

5’-CCGTGATAATGAGCAACACTATCGACATTCTTCAGAGTCTGACAATGAAG-3’

ΔC2-2

5’- AGTATCCTTCATTGTCAGACTCTGAAGAATGTCGATAGTGTTGCTCATTA-3’

These fusions resulted in the removal of amino acids 77-176 for Pk2-ΔPET, 77-382 for Pk2-ΔPETΔLIM, and 734-827 for Pk2-ΔC2.

Development ● Accepted manuscript

Dvl1-ΔPDZ$_{partial}$ was amplified by fusing 2 PCR products generated with the above and following primers:

5'-TGTAGCAGCGGATGGGCGTATTGAACCTATGGGCCCCTCCATGAGCATCATCACAT-3'

5'-ATGTGATGATGCTCATGGAGGGGCCCATAGGTTCAATACGCCCATCCGCTGCTACA-3'

This fusion resulted in the removal of amino acids 300-380.

Xenopus manipulations

Embryos were obtained and externally fertilized according to standard protocols (Sive *et al.* 1998). Developmental stages were determined according to Nieuwkoop and Faber (1967). For Pk2 morpholino treatments, 20-25ng was injected into one cell at the sixteen-cell stage for mosaic analysis or 30-35 ng at the four-cell stage, depending on experiment, and Pk2 was overexpressed at either 600-700pg or upwards of 1ng of mRNA similarly. About 22ng was injected for both Wdpcp/Fritz and Inturned morpholinos. Core PCP fluorescent protein fusion mRNA was injected into one of sixteen or thirty-two cells along with ~50pg of memRFP mRNA, with approximate amounts being 20-30pg for Dvl1-GFP, Dvl2-GFP, and Dvl3-GFP, 60-80pg Fzd6-GFP, Fzd7-GFP, and Fzd8-GFP, ~150pg for GFP/RFP-Pk2, and 50-60pg for GFP-Vangl1 and GFP-Vangl2. Pk2 deletion constructs were injected at 125-150pg for localization of GFP fused constructs and 700-800pg for overexpression of non-GFP fused constructs at the 16 cell stage. This amount was increased to 1ng at the 4-cell stage for the determination of effects on ciliary orientation. For Vangl1 and Dvl-ΔPDZ$_{partial}$ constructs injected at the 4 cell stage, 880pg were introduced. Centrin-RFP, CLAMP-GFP and GFP-Pk2 were co-injected into one of four cells at 60pg, 60pg, and 150pg, respectively.

Live Imaging and Confocal Image Quantification

All imaging was done using live embryos gently sandwiched between coverglasses using silicon grease as an adhesive spacer and carried out with a Zeiss LSM700 confocal microscope. Images were processed with the Fiji distribution of ImageJ, Imaris (Bitplane) and Photoshop (Adobe) software suites, and figures were assembled in Illustrator (Adobe). For PCP enrichment measures, freehand lines (3-5 pixels wide, depending on image zoom) were drawn over dorsoanterior and ventroposterior memRFP-labeled cell membranes with unlabeled neighbors on images in the Fiji distribution of ImageJ. Intensity measurements were then taken from these areas as well as from the GFP-PCP protein channel at the same area drawn. PCP enrichment was calculated by taking the natural log of the final value obtained after dividing the dorsoanterior measurements by the ventroposterior measurements,

Development • Accepted manuscript

both of which were normalized values of PCP-GFP average intensity divided by the membraneRFP intensity at the same region. Statistical analyses were carried out using Graphpad Prism software with Mann Whitney tests for significance. For FRAP analysis, time-lapse movies were acquired after simultaneously photobleaching anterior and posterior membrane domains of core PCP GFP fusions under control conditions and after previously described Pk2 overexpression and morpholino knockdown manipulations. Intensity measurements were performed in Fiji similarly to those take for PCP Enrichment, with recordings for each time point taken individually from each frame captured at bleached regions and normalized as detailed in (Goldman et al., 2005). Recovery trendlines were calculated and plotted in Graphpad Prism software with one phase exponential association curve fitting. Ciliary orientations were determined manually in Fiji, and Mean Polarity Vectors and Mean Vector lengths were calculated with the CircStat Matlab circular statistics toolbox (Berens, 2009) before values were plotted with Oriana software (Kovach Computing Services). For the assessment of flow across the epidermis, embryos were placed on modeling clay submerged in 1/3x MMR, and latex beads were loaded into the medium. Time-lapse imaging was performed using a Zeiss AXIO Zoom.V16 Stereomicroscope and associated Zen software. Movies were processed in Adobe Photoshop, and bead traces were performed manually with Fiji.

Development ● Accepted manuscript

Development • Accepted manuscript

Figures

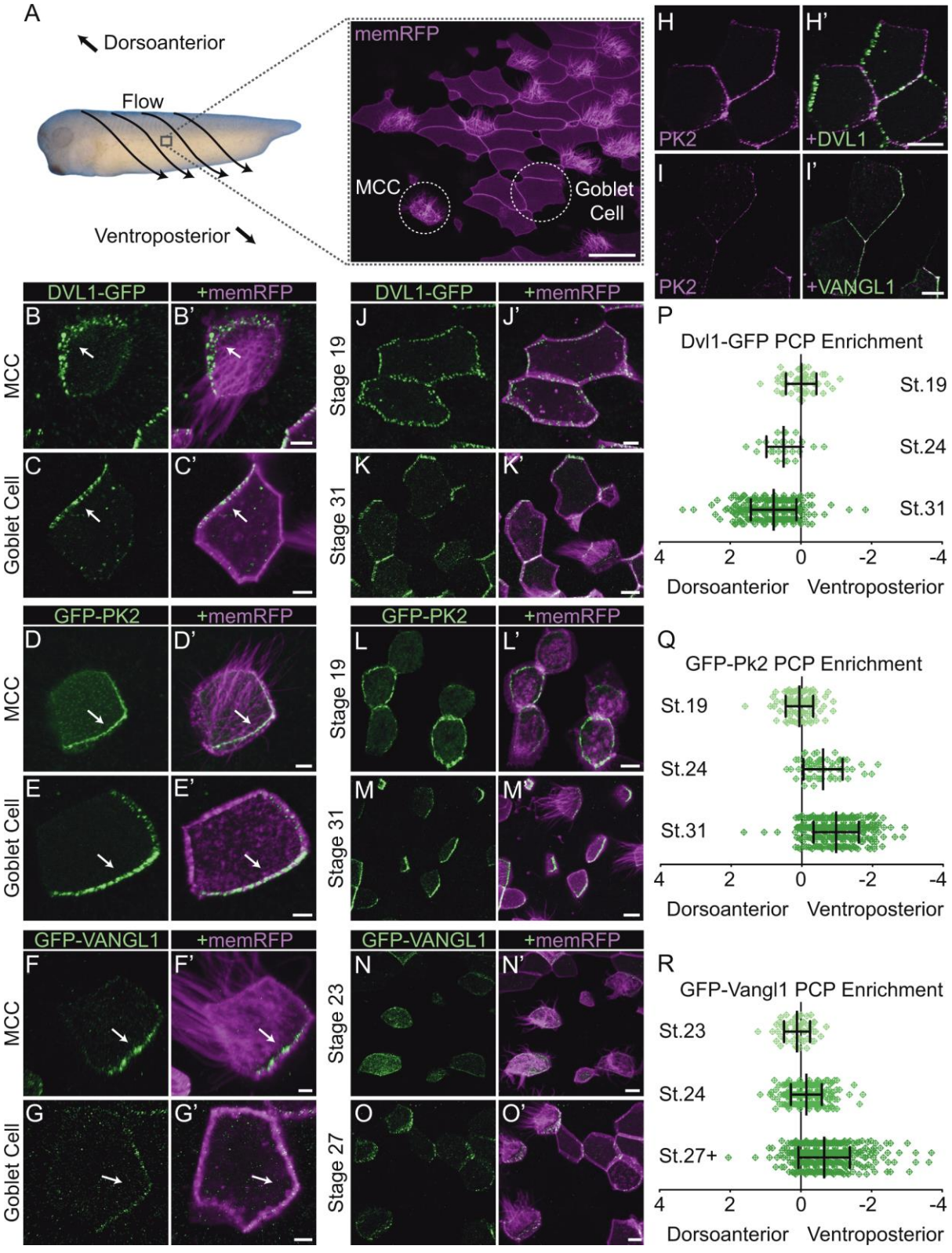

Figure 1. Core PCP proteins pattern the *Xenopus* epidermis during the refinement of basal body orientation.

(A) *Xenopus laevis* embryo with flow and anatomical directionality denoted along with a confocal slice showing different cell types visualized via membraneRFP in a mosaically-labeled epidermis. Scale represents 50µm.
(B-G) Multicilated cells (B,D,F) and goblet cells (C,E,G) in stage 31 embryo surrounded by unlabeled neighbors display asymmetric core PCP localization in the direction indicated by the overlying arrows. Scale represents 5µm.
(H,I) Groups of cells labeled with RFP-Pk2 and either mutually exclusive Dvl1-GFP (H) or co-localizing GFP-Vangl1 (I). Scale represents 10µm.
(J-M) Patches of cells mosaically labeled with either Dvl1-GFP (J,K) or GFP-Pk2 (L,M) at stages prior to ciliogenesis (St.19) and after basal body refinements (St.31). Scale represents 10µm.
(N,O) Patches of cells mosaically labeled with GFP-Vangl1 at stages during ciliogenesis (St.23) and during basal body refinement (St.27). Scale represents 10µm.
(P-R) Quantifications of PCP Enrichment at different developmental stages show increasing asymmetry develops during basal body refinement stages. Each mark represents the enrichment value for a single cell. All comparisons within graphs are highly significant ($p<0.0001$***) except for a modest increase between Dvl1 St.24 to St.31 ($p=0.0366$*).

Development ● Accepted manuscript

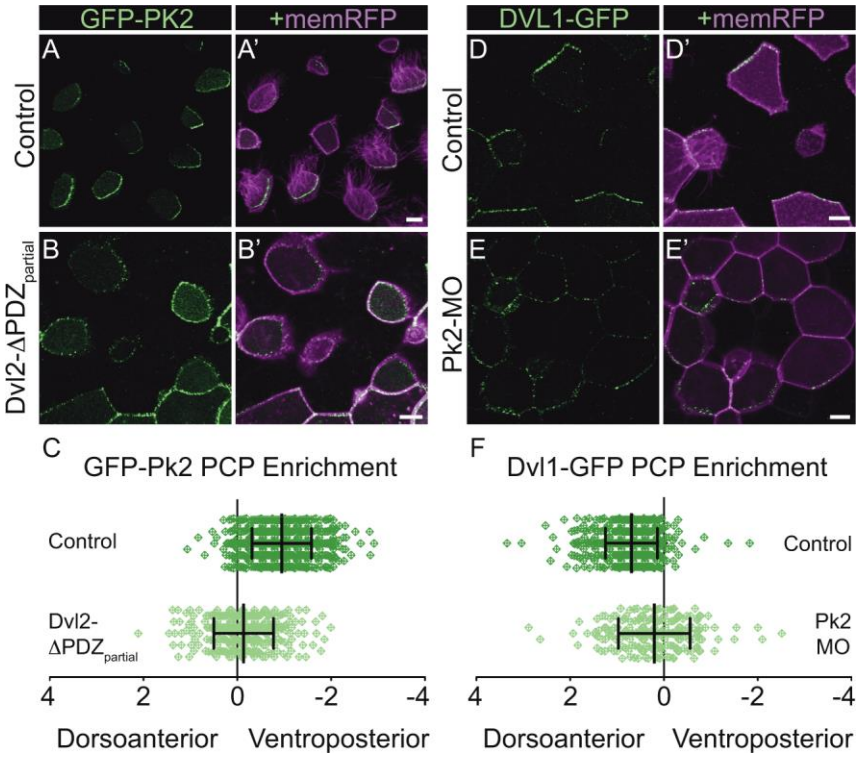

Figure 2. Intact PCP signaling is required for the formation of asymmetric core PCP complexes.

(A,B) Mosaically-labeled epidermal cells in St.31 *X.laevis* embryos have GFP-Pk2 localized asymmetrically in the control situation (A) and symmetrically upon overexpression of Xdd1 (B). Scale represents 10µm.
(C) Quantification of PCP Enrichment shows a significant shift upon Xdd1 expression ($p<0.0001$***).
(D,E) Mosaically-labeled epidermal cells in St.31 *X.laevis* embryos have GFP-Pk2 localized asymmetrically in the control situation (D) and symmetrically upon Pk2-MO knockdown (E). Scale represents 10µm .
(F) Quantification of PCP Enrichment shows a significant shift upon Pk2-MO knockdown ($p<0.0001$***).
(G,H) Mosaically-labeled epidermal cells in St.31 *X.laevis* embryos have GFP-Pk2 localized asymmetrically upon Intu-MO knockdown (G) and symmetrically upon WDPCP-MO knockdown (B). Scale represents 10µm.
(I) Quantification of PCP Enrichment shows a significant shift upon Intu-MO knockdown ($p=0.0031$**) and more significant shift upon Wdpcp-MO knockdown ($p<0.0001$***) in comparison to controls.

Development ● Accepted manuscript

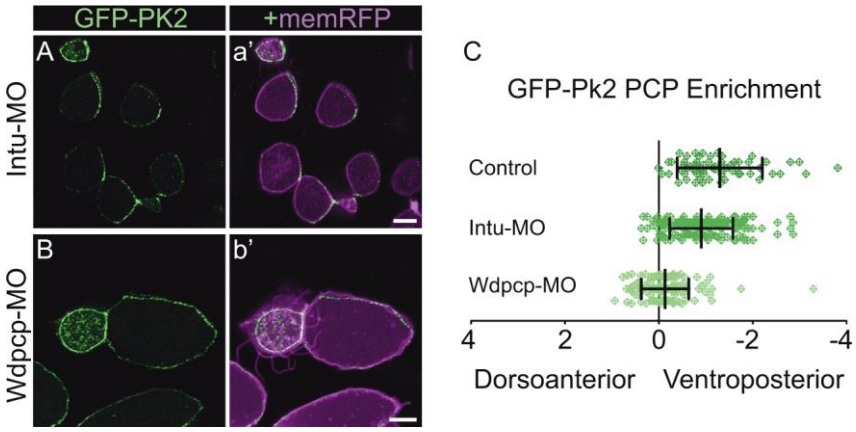

Figure 3. WDPCP knockdown disrupts core PCP patterning

(A,B) Mosaically-labeled epidermal cells in St.31 *X.laevis* embryos have GFP-Pk2 localized asymmetrically upon Intu-MO knockdown (A) and symmetrically upon WDPCP-MO knockdown (B). Scale represents 10μm. **(C)** Quantification of PCP Enrichment shows a significant shift upon Intu-MO knockdown ($p=0.0031^{**}$) and more significant shift upon Wdpcp-MO knockdown ($p<0.0001^{***}$) in comparison to controls.

Development ● Accepted manuscript

Development ● Accepted manuscript

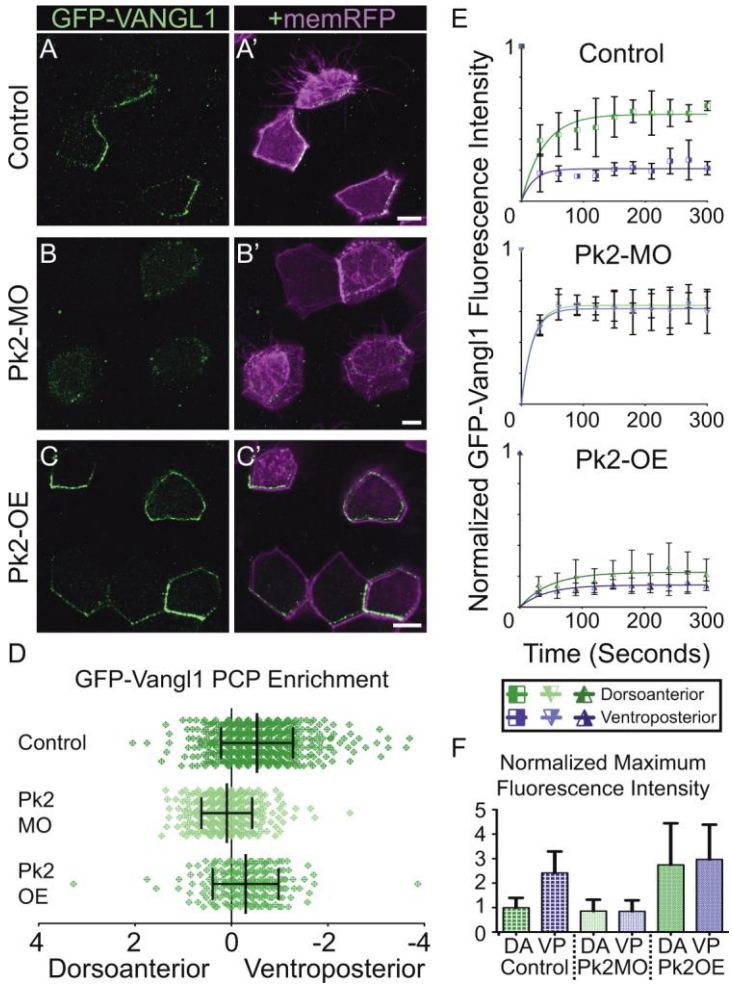

Figure 4. Pk2 expression levels influence the dynamic localization of apicolateral Vangl1 accumulations.

(A-C) Mosaically-labeled epidermal cells in St.31 *X.laevis* embryos have GFP-Vangl1 localized asymmetrically in the control situation (A), absent from apicolateral enrichments upon Pk2-MO knockdown (B) and localized more symmetrically with Pk2 overexpression (C). Scale represents 10μm.
(D) Quantification of PCP Enrichment shows a significant shift upon Pk2-MO knockdown ($p<0.0001$***) and Pk2 overexpression ($p=0.0002$***) in comparison to controls.
(E) Graphs depicting recovery trends of GFP-Vangl1 fluorescence intensity following simultaneous bleaching at discrete dorsoanterior (green lines) and ventroposterior (purple lines) cortical regions in stage 25 embryos (FRAP). Scale bars represent the standard error of the mean (SEM) from 3 separately bleached cells in 2-3 different embryos.
(F) Comparison of the maximum fluorescence intensities at regions measured in (E) prior to bleaching, which are normalized to dorsoanterior intensity in the control situation.

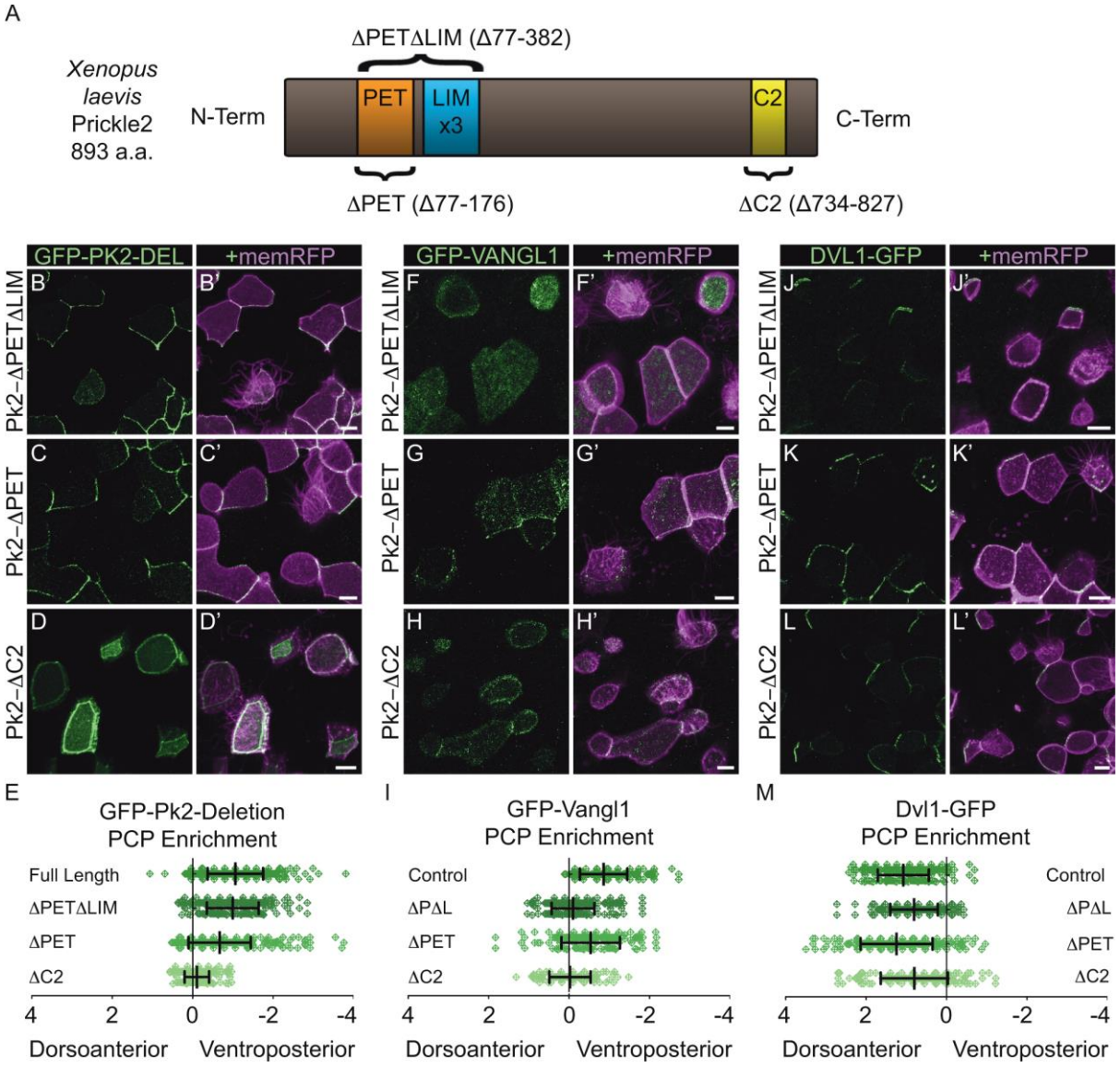

Figure 5. The Pk2 C2 domain is required for Pk2 asymmetry, while both the LIM and C2 domains promote the asymmetric enrichment of Vangl1.

(A) Schematic of *X.laevis* Prickle2 and location of conserved domains removed from Pk2 deletion constructs.
(B-D) Cellular localizations of GFP-Pk2 with sequence deletions that correspond to the PET and LIM domains (B), PET domain alone (C), and C-terminal region C2 (D). Scale represents 10μm.
(E) Graph depicting changes in localization of Pk2 caused by conserved domain deletions, with the normal localization of GFP-Pk2-ΔPETΔLIM (ns, p=0.4037), still asymmetric yet significantly misaligned GFP-Pk2-ΔPET (p<0.0001***), and symmetric GFP-Pk2-ΔC2 (p<0.0001***).
(F-H) Cellular localizations of GFP-Vangl1 upon the overexpression of Pk2-ΔPETΔLIM (F), Pk2-ΔPET (G), and Pk2-ΔC2 (H). Scale represents 10μm.
(I) Graph depicting changes in localization of Vangl1 caused by overexpression of Pk2 deletions, with a loss of asymmetry upon Pk2-ΔPETΔLIM and Pk2-ΔC2 overexpression (p<0.0001***) and significant reduction upon Pk2-ΔPET overexpression (p=0.0001***).
(J-L) Cellular localizations of Dvl1-GFP upon the overexpression of Pk2-ΔPETΔLIM (J), Pk2-ΔPET (K), and Pk2-ΔC2 (L). Scale represents 10μm.
(M) Graph depicting changes in localization of Dvl1 caused by overexpression of Pk2 deletions, with a significant shift in but not loss of asymmetric enrichment upon Pk2-ΔPETΔLIM (p<0.0001***), Pk2-ΔPET (p=0.0181*), and Pk2-ΔC2 overexpression (p=0.0002***).

Development ● Accepted manuscript

Development ● Accepted manuscript

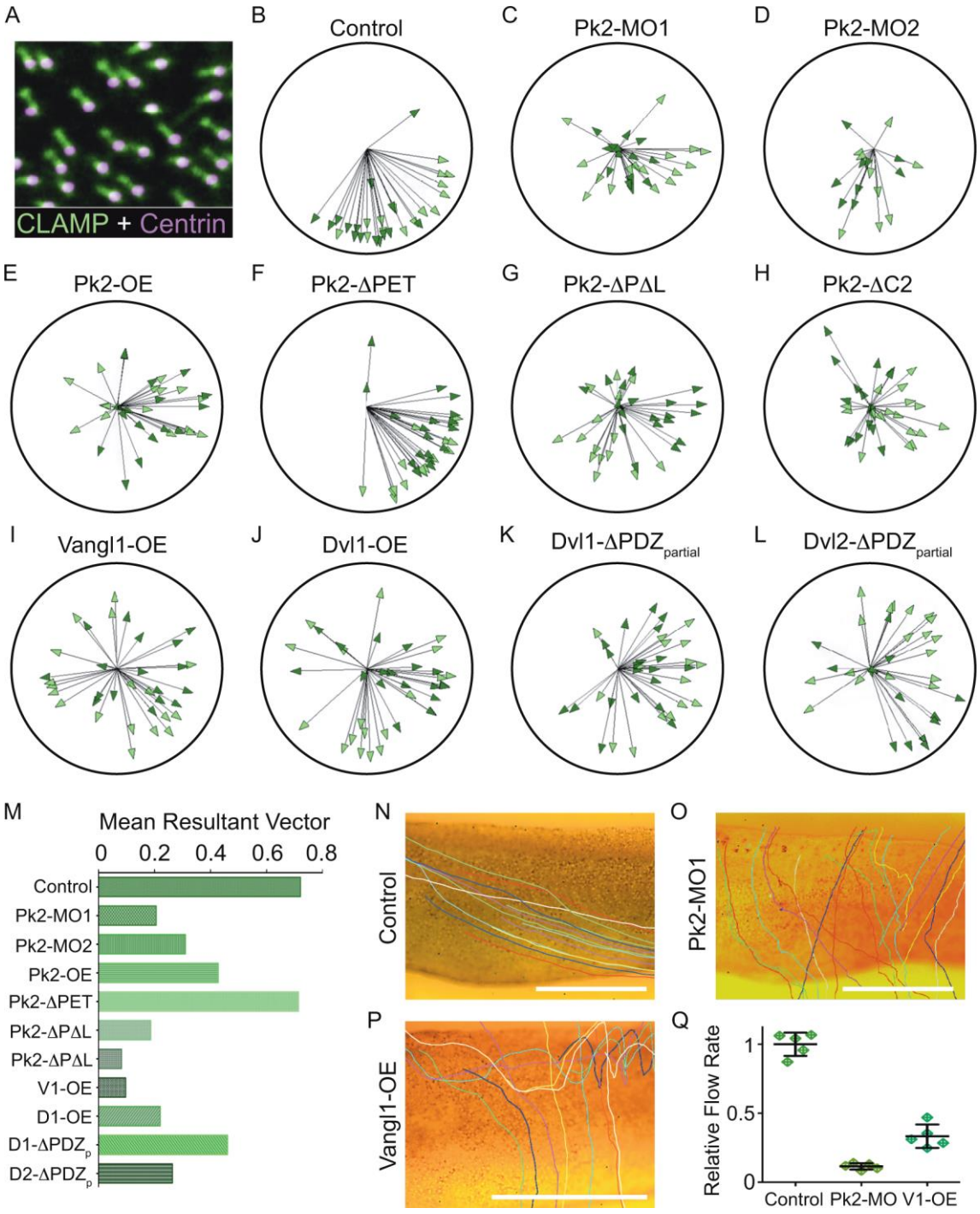

Figure 6. Disrupting PCP patterning leads to structural defects in basal body polarity

(A) Apical intercellular region of a single MCC labeled with CLAMP-GFP and Centrin-RFP, which when combined display the orientation of cilia in respect to the direction of ciliary beating (CLAMP points the opposite direction).

(B-L) Plots displaying the mean basal body orientation and associated mean vector length of MCCs under various experimental conditions. Each arrow represents a measure of the orientations of a single MCC, with increased length correlated with less variation between basal bodies within each MCC. Dark and light arrowheads represent data from separate experimental repeats, with each experiment involving measures from at least 5 cells from at least 3 embryos each. The combined data is displayed for control (B), Pk2-MO#1 knockdown (C), Pk2-MO#2 knockdown (D), Pk2 overexpression (E), Pk2-ΔPET overexpression (F), Pk2-

ΔPETΔLIM overexpression (G), Pk2-ΔC2 overexpression (H), Vangl1 overexpression (I), Dvl1 overexpression (J), Dvl1-$\Delta PDZ_{partial}$ overexpression (K), and Dvl2-$\Delta PDZ_{partial}$ (Xdd1) overexpression (L) conditions.
(M) Graph illustrating the mean resultant vector length from the combined measurements for all MCCs across all embryos from both experimental treatments , serving as an overall metric for PCP disruption.
(N-P) Stills from the end of movies showing the traces of beads carried by flow across the epidermis of stage 31 *Xenopus laevis* embryos that have been uninjected (N) or injected with either Pk2-MO (O) or a high dose of Vangl1 mRNA (P).
(Q) Quantification of the flow rate from 5 beads traced in the movies from which the final frame is shown in (N-P).

Development ● Accepted manuscript

Acknowledgements

The authors would like to thank A. Shindo, J. Tabler, and our reviewers for critcal reading of the manuscript. We would like to thank Peter Klein for Fzd8-GFP and Herbert Steinbeisser for Fzd7-GFP plasmids. This work was supported by grants to from the NIGMS and NHLBI to J.B.W. J.B.W. is an Ealery Career Scientist of HHMI.

Development ● Accepted manuscript

Development • Accepted manuscript

References

Adler, P. N. (1992). The genetic control of tissue polarity in Drosophila. *Bioessays* **14**, 735–741.

Adler, P. N., Krasnow, R. E. and Lui, J. (1997). Tissue polarity points from cells that have higher Frizzled levels towards cells that have lower Frizzled levels. *Current Biology* **7**, 940–949.

Adler, P. N., Taylor, J. and Charlton, J. (2000). The domineering non-autonomy of frizzled and van Gogh clones in the Drosophila wing is a consequence of a disruption in local signaling. *Mech Dev* **96**, 197–207.

Aigouy, B., Farhadifar, R., Staple, D. B., Sagner, A., Röper, J.-C., Jülicher, F. and Eaton, S. (2010). Cell Flow Reorients the Axis of Planar Polarity in the Wing Epithelium of Drosophila. *Cell* **142**, 773–786.

Amonlirdviman, K., Khare, N. A., Tree, D. R. P., Chen, W.-S., Axelrod, J. D. and Tomlin, C. J. (2005). Mathematical modeling of planar cell polarity to understand domineering nonautonomy. *Science* **307**, 423–426.

Axelrod, J. D. (2001). Unipolar membrane association of Dishevelled mediates Frizzled planar cell polarity signaling. *Genes & Development* **15**, 1182–1187.

Bastock, R., Strutt, H. and Strutt, D. (2003). Strabismus is asymmetrically localised and binds to Prickle and Dishevelled during Drosophila planar polarity patterning. *Development* **130**, 3007–3014.

Berens, P. (2009). CircStat: A MATLAB Toolbox for Circular Statistics. **31**, 1–21.

Billett, F. S. and Gould, R. P. (1971). Fine structural changes in the differentiating epidermis of Xenopus laevis embryos. *J Anat* **108**, 465–480.

Boutin, C., Labedan, P., Dimidschstein, J., Richard, F., Cremer, H., Andre, P., Yang, Y., Montcouquiol, M., Goffinet, A. M. and Tissir, F. (2014). A dual role for planar cell polarity genes in ciliated cells. *Proceedings of the National Academy of Sciences*.

Brooks, E. R. and Wallingford, J. B. (2014). Multiciliated Cells. *Curr Biol* **24**, R973–R982.

Chen, W.-S., Antic, D., Matis, M., Logan, C. Y., Povelones, M., Anderson, G. A., Nusse, R. and Axelrod, J. D. (2008). Asymmetric Homotypic Interactions of the Atypical Cadherin Flamingo Mediate Intercellular Polarity Signaling. *Cell* **133**, 1093–1105.

Cho, B., Pierre-Louis, G., Sagner, A., Eaton, S. and Axelrod, J. D. (2015). Clustering and Negative Feedback by Endocytosis in Planar Cell Polarity Signaling Is Modulated by Ubiquitinylation of Prickle. *PLoS Genet* **11**, e1005259.

Chung, M. I., Kwon, T., Tu, F., Brooks, E. R., Gupta, R., Meyer, M., Baker, J. C., Marcotte, E. M. and Wallingford, J. B. (2014). Coordinated genomic control of ciliogenesis and cell movement by RFX2. *eLife* **3**, e01439–e01439.

Collier, S., Lee, H., Burgess, R. and Adler, P. (2005). The WD40 Repeat Protein Fritz

Development ● Accepted manuscript

Links Cytoskeletal Planar Polarity to Frizzled Subcellular Localization in the Drosophila Epidermis. *Genetics* **169**, 2035–2045.

Cui, C., Chatterjee, B., Lozito, T. P., Zhang, Z., Francis, R. J., Yagi, H., Swanhart, L. M., Sanker, S., Francis, D., Yu, Q., et al. (2013). Wdpcp, a PCP Protein Required for Ciliogenesis, Regulates Directional Cell Migration and Cell Polarity by Direct Modulation of the Actin Cytoskeleton. *PLoS Biol* **11**, e1001720.

Das, G., Jenny, A., Klein, T. J., Eaton, S. and Mlodzik, M. (2004). Diego interacts with Prickle and Strabismus/Van Gogh to localize planar cell polarity complexes. *Development* **131**, 4467–4476.

Daulat, A. M., Luu, O., Sing, A., Zhang, L., Wrana, J. L., McNeill, H., Winklbauer, R. and Angers, S. (2011). Mink1 regulates beta-catenin-independent Wnt signaling via Prickle phosphorylation. *Molecular and Cellular Biology* **32**, 173–185.

Deans, M. R., Antic, D., Suyama, K., Scott, M. P., Axelrod, J. D. and Goodrich, L. V. (2007). Asymmetric Distribution of Prickle-Like 2 Reveals an Early Underlying Polarization of Vestibular Sensory Epithelia in the Inner Ear. *Journal of Neuroscience* **27**, 3139–3147.

Drysdale, T. A. and Elinson, R. P. (1992). Cell migration and induction in the development of the surface ectodermal pattern of the Xenopus laevis tadpole. *Develop. Growth Differ.* **34**, 51–59.

Dubaissi, E. and Papalopulu, N. (2011). Embryonic frog epidermis: a model for the study of cell-cell interactions in the development of mucociliary disease. *Disease Models & Mechanisms* **4**, 179–192.

Dubaissi, E., Rousseau, K., Lea, R., Soto, X., Nardeosingh, S., Schweickert, A., Amaya, E., Thornton, D. J. and Papalopulu, N. (2014). A secretory cell type develops alongside multiciliated cells, ionocytes and goblet cells, and provides a protective, anti-infective function in the frog embryonic mucociliary epidermis. *Development* **141**, 1514–1525.

Goldman, R. D., Spector, D. L. and Swedlund, A. C. (2005). *Live cell imaging: a laboratory manual*. Cold Spring Harbor Laboratory Press Cold Spring Harbor, NY:.

Goodrich, L. V. and Strutt, D. (2011). Principles of planar polarity in animal development. *Development* **138**, 1877–1892.

Gray, R. S., Abitua, P. B., Wlodarczyk, B. J., Szabo-Rogers, H. L., Blanchard, O., Lee, I., Weiss, G. S., Liu, K. J., Marcotte, E. M., Wallingford, J. B., et al. (2009). The planar cell polarity effector Fuz is essential for targeted membrane trafficking, ciliogenesis and mouse embryonic development. *Nature Cell Biology* **11**, 1225–1232.

Gray, R. S., Roszko, I. and Solnica-Krezel, L. (2011). Planar Cell Polarity:Coordinating Morphogenetic Cell Behaviors with Embryonic Polarity. *Developmental Cell* **21**, 120–133.

Gubb, D. (1993). Genes controlling cellular polarity in Drosophila. *Dev Suppl* 269–277.

Gubb, D. and Garcia-Bellido, A. (1982). A genetic analysis of the determination of cuticular polarity during development in Drosophila melanogaster. *J Embryol Exp Morphol* **68**, 37–57.

Guirao, B., Meunier, A., Mortaud, S., Aguilar, A., Corsi, J.-M., Strehl, L., Hirota, Y., Desoeuvre, A., Boutin, C., Han, Y.-G., et al. (2010). Coupling between hydrodynamic forces and planar cell polarity orients mammalian motile cilia. *Nature Cell Biology* **12**, 341–350.

Guo, Y., Zanetti, G. and Schekman, R. (2013). A novel GTP-binding protein-adaptor protein complex responsible for export of Vangl2 from the trans Golgi network. *eLife* **2**, e00160–e00160.

Jakobsen, L., Vanselow, K., Skogs, M., Toyoda, Y., Lundberg, E., Poser, I., Falkenby, L. G., Bennetzen, M., Westendorf, J., Nigg, E. A., et al. (2011). Novel asymmetrically localizing components of human centrosomes identified by complementary proteomics methods. *The EMBO Journal* **30**, 1520–1535.

Jenny, A., Darken, R. S., Wilson, P. A. and Mlodzik, M. (2003). Prickle and Strabismus form a functional complex to generate a correct axis during planar cell polarity signaling. *The EMBO Journal* **22**, 4409–4420.

Jenny, A., Reynolds-Kenneally, J., Das, G., Burnett, M. and Mlodzik, M. (2005). Diego and Prickle regulate Frizzled planar cell polarity signalling by competing for Dishevelled binding. *Nature Cell Biology* **7**, 691–697.

Kim, S. K., Shindo, A., Park, T. J., Oh, E. C., Ghosh, S., Gray, R. S., Lewis, R. A., Johnson, C. A., Attie-Bittach, T., Katsanis, N., et al. (2010). Planar Cell Polarity Acts Through Septins to Control Collective Cell Movement and Ciliogenesis. *Science* **329**, 1337–1340.

König, G. and Hausen, P. (1993). Planar Polarity in the Ciliated Epidermis of *Xenopus* Embryos. *Developmental Biology* **160**, 355–368.

Lee, H. and Adler, P. N. (2002). The function of the frizzled pathway in the Drosophila wing is dependent on inturned and fuzzy. *Genetics* **160**, 1535–1547.

Lin, Y.-Y. and Gubb, D. (2009). Molecular dissection of Drosophila Prickle isoforms distinguishes their essential and overlapping roles in planar cell polarity. *Developmental Biology* **325**, 386–399.

Liu, C., Lin, C., Gao, C., May-Simera, H., Swaroop, A. and Li, T. (2014). Null and hypomorph Prickle1 alleles in mice phenocopy human Robinow syndrome and disrupt signaling downstream of Wnt5a. *Biology Open*.

Merte, J., Jensen, D., Wright, K., Sarsfield, S., Wang, Y., Schekman, R. and Ginty, D. D. (2009). Sec24b selectively sorts Vangl2 to regulate planar cell polarity during neural tube closure. *Nature Cell Biology* **12**, 41–46.

Mitchell, B., Jacobs, R., Li, J., Chien, S. and Kintner, C. (2007). A positive feedback mechanism governs the polarity and motion of motile cilia. *Nature* **447**, 97–101.

Development ● Accepted manuscript

Mitchell, B., Stubbs, J. L., Huisman, F., Taborek, P., Yu, C. and Kintner, C. (2009). The PCP Pathway Instructs the Planar Orientation of Ciliated Cells in the Xenopus Larval Skin. *Current Biology* **19**, 924–929.

Narimatsu, M., Bose, R., Pye, M., Zhang, L., Miller, B., Ching, P., Sakuma, R., Luga, V., Roncari, L., Attisano, L., et al. (2009). Regulation of Planar Cell Polarity by Smurf Ubiquitin Ligases. *Cell* **137**, 295–307.

Okumura, A., Yamamoto, T., Miyajima, M., Shimojima, K., Kondo, S., Abe, S., Ikeno, M. and Shimizu, T. (2014). 3p Interstitial Deletion Including PRICKLE2 in Identical Twins With Autistic Features. *Pediatr Neurol*.

Park, T. J., Haigo, S. L. and Wallingford, J. B. (2006). Ciliogenesis defects in embryos lacking inturned or fuzzy function are associated with failure of planar cell polarity and Hedgehog signaling. *Nature Genetics* **38**, 303–311.

Park, T. J., Mitchell, B. J., Abitua, P. B., Kintner, C. and Wallingford, J. B. (2008). Dishevelled controls apical docking and planar polarization of basal bodies in ciliated epithelial cells. *Nature Genetics* **40**, 871–879.

Quigley, I. K., Stubbs, J. L. and Kintner, C. (2011). Specification of ion transport cells in the Xenopus larval skin. *Development* **138**, 705–714.

Seifert, J. R. K. and Mlodzik, M. (2007). Frizzled/PCP signalling: a conserved mechanism regulating cell polarity and directed motility. *Nat Rev Genet* **8**, 126–138.

Sokol, S. Y. (1996). Analysis of Dishevelled signalling pathways during Xenopus development. *Curr Biol* **6**, 1456–1467.

Song, H., Hu, J., Chen, W., Elliott, G., Andre, P., Gao, B. and Yang, Y. (2010). Planar cell polarity breaks bilateral symmetry by controlling ciliary positioning. *Nature* **466**, 378–382.

Sowers, L. P., Loo, L., Wu, Y., Campbell, E., Ulrich, J. D., Wu, S., Paemka, L., Wassink, T., Meyer, K., Bing, X., et al. (2013). Disruption of the non-canonical Wnt gene PRICKLE2 leads to autism-like behaviors with evidence for hippocampal synaptic dysfunction. *Mol Psychiatry* **18**, 1077–1089.

Struhl, G., Casal, J. and Lawrence, P. A. (2012). Dissecting the molecular bridges that mediate the function of Frizzled in planar cell polarity. *Development* **139**, 3665–3674.

Strutt, D. (2008). The planar polarity pathway. *Curr Biol* **18**, R898–R902.

Strutt, D. and Strutt, H. (2007). Differential activities of the core planar polarity proteins during Drosophila wing patterning. *Developmental Biology* **302**, 181–194.

Strutt, D. I. (2001). Asymmetric localization of frizzled and the establishment of cell polarity in the Drosophila wing. *Molecular Cell* **7**, 367–375.

Strutt, H. and Strutt, D. (2002). Nonautonomous planar polarity patterning in Drosophila: dishevelled-independent functions of frizzled. *Developmental Cell* **3**, 851–863.

Development ● Accepted manuscript

Strutt, H. and Strutt, D. (2008). Differential Stability of Flamingo Protein Complexes Underlies the Establishment of Planar Polarity. *Current Biology* **18**, 1555–1564.

Strutt, H. and Strutt, D. (2009). Asymmetric localisation of planar polarity proteins: Mechanisms and consequences. *Seminars in Cell and Developmental Biology* **20**, 957–963.

Strutt, H., Searle, E., Thomas-MacArthur, V., Brookfield, R. and Strutt, D. (2013a). A Cul-3-BTB ubiquitylation pathway regulates junctional levels and asymmetry of core planar polarity proteins. *Development* **140**, 1693–1702.

Strutt, H., Thomas-MacArthur, V. and Strutt, D. (2013b). Strabismus Promotes Recruitment and Degradation of Farnesylated Prickle in Drosophila melanogaster Planar Polarity Specification. *PLoS Genet* **9**, e1003654.

Strutt, H., Warrington, S. J. and Strutt, D. (2011). Dynamics of Core Planar Polarity Protein Turnover and Stable Assemblyinto Discrete Membrane Subdomains. *Developmental Cell* **20**, 511–525.

Sweede, M., Ankem, G., Chutvirasakul, B., Azurmendi, H. F., Chbeir, S., Watkins, J., Helm, R. F., Finkielstein, C. V. and Capelluto, D. G. S. (2008). Structural and Membrane Binding Properties of the Prickle PET Domain †. *Biochemistry* **47**, 13524–13536.

Takeuchi, M., Nakabayashi, J., Sakaguchi, T., Yamamoto, T. S., Takahashi, H., Takeda, H. and Ueno, N. (2003). The prickle-Related Gene in Vertebrates Is Essential for Gastrulation Cell Movements. *Current Biology* **13**, 674–679.

Tao, H., Manak, J. R., Sowers, L., Mei, X., Kiyonari, H., Abe, T., Dahdaleh, N. S., Yang, T., Wu, S., Chen, S., et al. (2011). Mutations in prickle orthologs cause seizures in flies, mice, and humans. *The American Journal of Human Genetics* **88**, 138–149.

Torban, E., Patenaude, A.-M., Leclerc, S., Rakowiecki, S., Gauthier, S., Andelfinger, G., Epstein, D. J. and Gros, P. (2008). Genetic interaction between members of the Vangl family causes neural tube defects in mice. *Proc Natl Acad Sci U S A* **105**, 3449–3454.

Tree, D. R. P., Shulman, J. M., Rousset, R., Scott, M. P., Gubb, D. and Axelrod, J. D. (2002). Prickle mediates feedback amplification to generate asymmetric planar cell polarity signaling. *Cell* **109**, 371–381.

Twitty, V. C. (1928). Experimental studies on the ciliary action of amphibian embryos. *J. Exp. Zool.* **50**, 319–344.

Vinson, C. R. and Adler, P. N. (2002). Directional non-cell-autonomy and the transmission of polarity information by the *frizzled* gene of *Drosophila*. *Nature* **329**, 549–551.

Vladar, E. K., Bayly, R. D., Sangoram, A. M., Scott, M. P. and Axelrod, J. D. (2012). Microtubules Enablethe Planar Cell Polarity of Airway Cilia. *Current Biology* 1–10.

Walentek, P., Bogusch, S., Thumberger, T., Vick, P., Dubaissi, E., Beyer, T., Blum, M. and Schweickert, A. (2014). A novel serotonin-secreting cell type regulates ciliary motility in the mucociliary epidermis of Xenopus tadpoles. *Development* **141**, 1526–

Development ● Accepted manuscript

1533.

Wallingford, J. B. (2010). Planar cell polarity signaling, cilia and polarized ciliary beating. *Current Opinion in Cell Biology* **22**, 597–604.

Wallingford, J. B. (2012). Planar Cell Polarity and the Developmental Control of Cell Behavior in Vertebrate Embryos. *Annu. Rev. Cell Dev. Biol.* **28**, 627–653.

Wallingford, J. B., Rowning, B. A., Vogeli, K. M., Rothbacher, U., Fraser, S. E. and Harland, R. M. (2000). Dishevelled controls cell polarity during Xenopus gastrulation. *Nature* **405**, 81–85.

Wang, Y., Yan, J., Lee, H., Lu, Q. and Adler, P. N. (2014). The proteins encoded by the Drosophila Planar Polarity Effector genes inturned, fuzzy and fritz interact physically and can re-pattern the accumulation of "upstream" Planar Cell Polarity proteins. *Developmental Biology* **394**, 156–169.

Wen, S., Zhu, H., Lu, W., Mitchell, L. E., Shaw, G. M., Lammer, E. J. and Finnell, R. H. (2010). Planar cell polarity pathway genes and risk for spina bifida. *Am. J. Med. Genet.* **152A**, 299–304.

Werner, M. E., Hwang, P., Huisman, F., Taborek, P., Yu, C. C. and Mitchell, B. J. (2007). Actin and microtubules drive differential aspects of planar cell polarity in multiciliated cells. *Annu Rev Physiol* **195**, 423–450.

Wong, L. L. and Adler, P. N. (1993). Tissue polarity genes of Drosophila regulate the subcellular location for prehair initiation in pupal wing cells. *The Journal of Cell Biology* **123**, 209–221.

Wu, J. and Mlodzik, M. (2008). The Frizzled Extracellular Domain Is a Ligand for Van Gogh/Stbm during Nonautonomous Planar Cell Polarity Signaling. *Developmental Cell* **15**, 462–469.

Yin, H., Copley, C. O., Goodrich, L. V. and Deans, M. R. (2012). Comparison of Phenotypes between Different vangl2 Mutants Demonstrates Dominant Effects of the Looptail Mutation during Hair Cell Development. *PLoS ONE* **7**, e31988.

Zeng, H., Hoover, A. N. and Liu, A. (2010). PCP effector gene Inturned is an important regulator of cilia formation and embryonic development in mammals. *Developmental Biology* **339**, 418–428.

Development ● Accepted manuscript

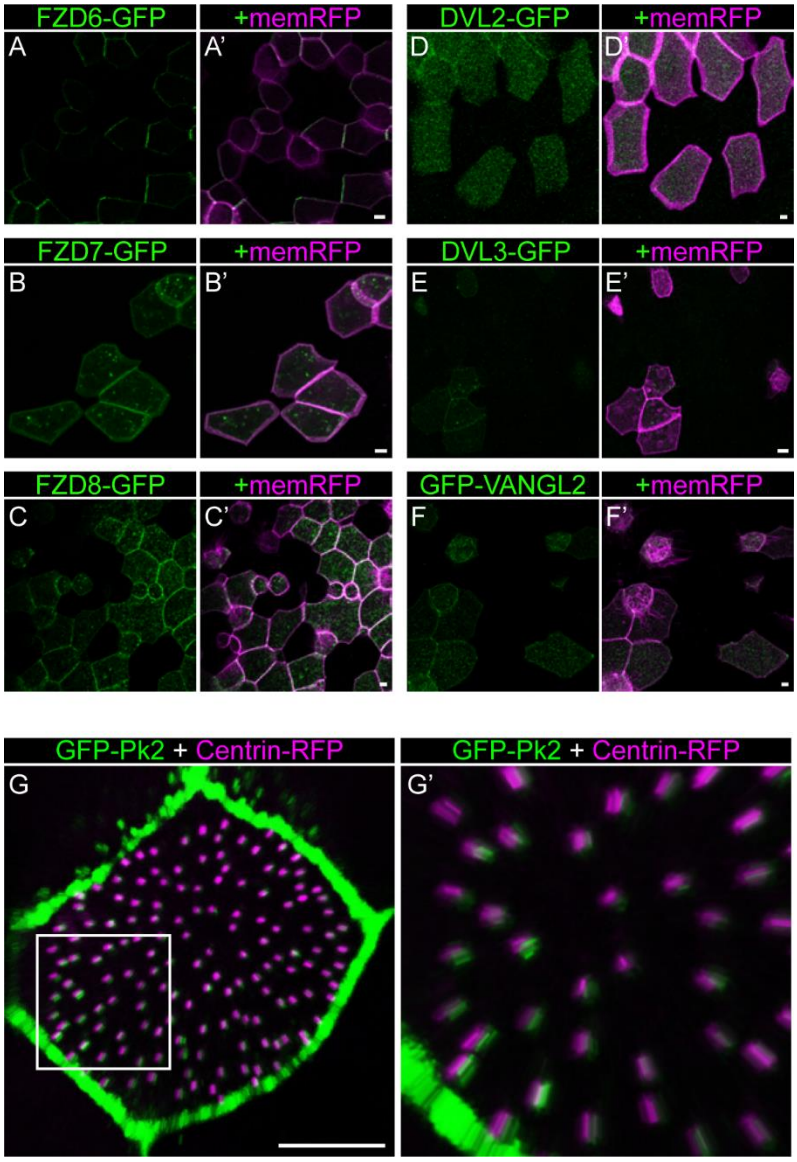

Fig. S1. Alternate Core PCP family members differentially localize in the *Xenopus* epidermis. (A-F) Mosaically-labeled cells in stage 31 embryos labeled with PCP proteins fused to GFP and membraneRFP and surrounded by unlabeled neighbors. Frizzled-6 (A) displays asymmetric localization while Frizzled-7 (B), Frizzled-8 (C), Dishevelled-2 (D), Dishevelled-3 (E), and Vangl2 (F) all decorate the cortex in a symmetrical fashion. Scale represents 10μm. (G) GFP-Pk2 assumes a polarized localization near basal bodies labeled with Centrin-RFP after the finalization of basal orientation refinement (St.35 shown). Note that this cell is surrounded by similarly labeled cells, making the Pk2 cortical asymmetry unapparent. Box in (G) demarcates the area magnified in (G′). Scale bar represents 10μm.

Development • Supplementary information

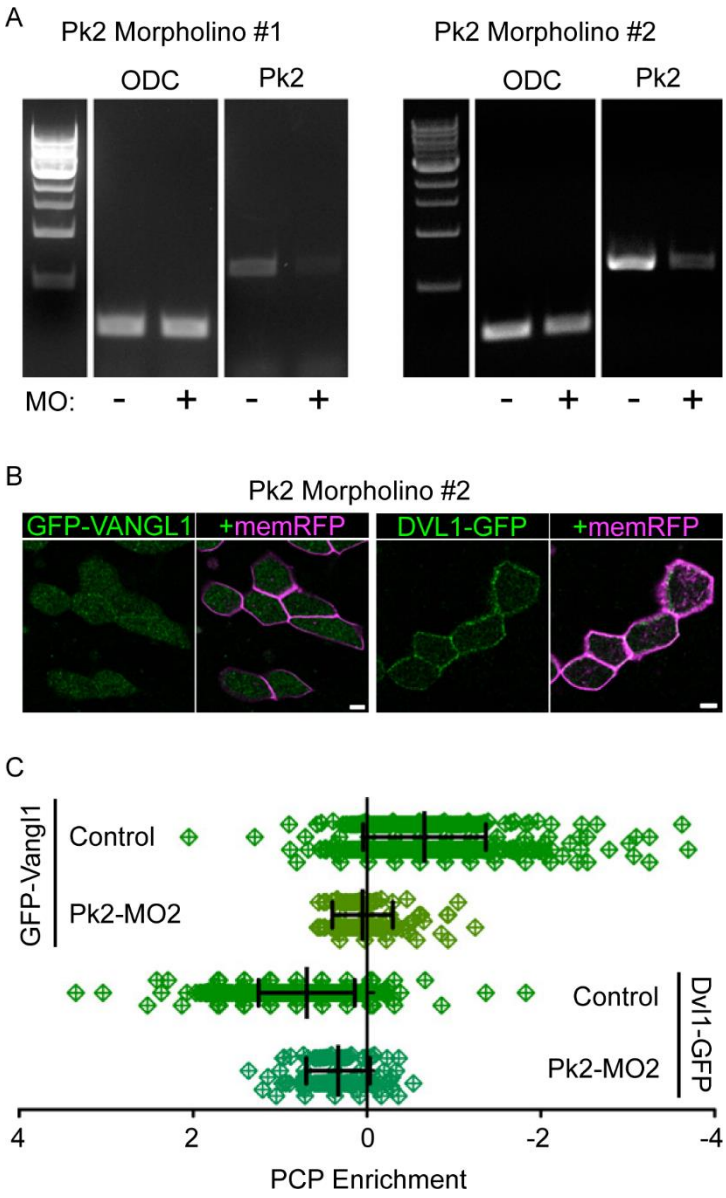

Fig. S2. Pk2 morpholinos reduce Pk2 mRNA levels, resulting in a reduction of Dvl1 and Vang1 asymmetry. (A) RT-PCR results for the amplification of a control, ornithine decarboxylase (ODC), and morpholino-targeted Pk2 sequence from cDNA of embryos that were either uninjected or injected with Pk2 morpholino #1 or #2 into 4 of 4 cells, demonstrating a significant reduction of only the Pk2 PCR product in morpholino-injected embryos. (B) Cells in stage 31 embryos labeled with PCP proteins fused to GFP and membraneRFP with an included dose of Pk2 morpholino #2, showing similar effects to Pk2 morpholino #1 shown in Fig.s 2 and 4. Scale bars represent 10μm. (C) Graph depicting changes in localization of Vangl1 and Dvl1 caused by Pk2 knockdown with a second Pk2 morpholino (Pk2-MO#2) targeting an alternative splicing site from the first. PCP enrichment is significantly reduced for both GFP-Vangl1 ($p<0.0001$***) and Dvl1-GFP ($p<0.0001$***) in morphant cells (n= 137 for Vangl1 and 131 for Dvl1) in comparison to controls (n= 519 cells for Vangl1 and 508 cells for Dvl1). Error bars indicate standard deviation of the mean.

Development • Supplementary information

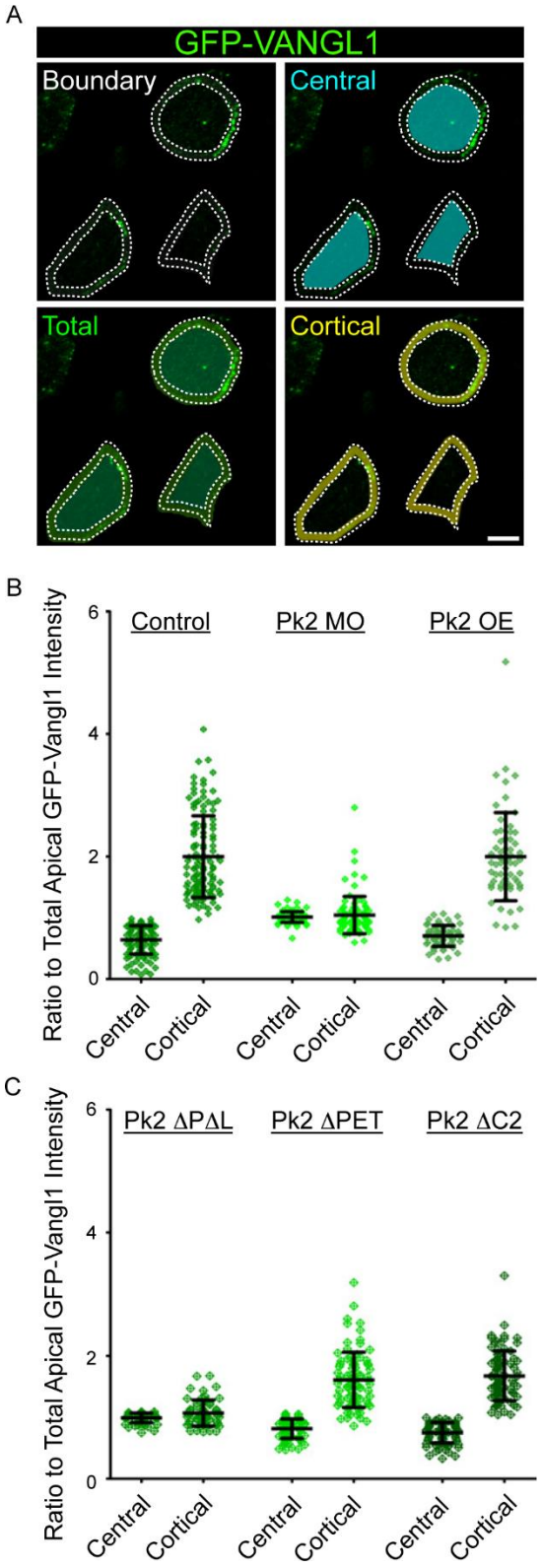

Fig. S3. GFP-Vangl1 Enrichment is abolished upon Pk2 MO knockdown and Pk2-ΔPETΔLIM overexpression. (A) Schematic of quantification method of data presented in (B,C). Either the average cortical fluorescence intensity or the average intensity of the remaining central area within each cell was

Development • Supplementary information

divided by the average fluorescence intensity of the total apical surface area (both regions combined). Scale represents 10μm. (B) Quantification data showing a significant loss of cortical enrichment of GFP-Vangl1 upon Pk2-MO knockdown. Each dot represents one cell, and each cell has both a Central and a Cortical quotient presented with the total apical fluorescence measure as the divisor. Combined, these two measurements are highly significant from another in the control (n= 123) and Pk2-OE (n=63) conditions ($p<0.0001$***) but not significant for Pk2-MO knockdown (n=94) ($p=0.2854$). Error bars indicate Standard deviation of the mean. (C) Quantification data showing a significant loss of cortical enrichment of GFP-Vangl1 upon overexpression of Pk2-ΔPETΔLIM. Each dot represents one cell, and each cell has both a Central and a Cortical measurement as presented in (B). Combined, these two measurements are highly significant from another in the Pk2-ΔPET (n= 85) and Pk2-ΔC2 (n= 84) conditions ($p<0.0001$***) but not significant for Pk2-ΔPETΔLIM (n=58) ($p=0.1519$). Error bars indicate standard deviation of the mean.

Development • Supplementary information

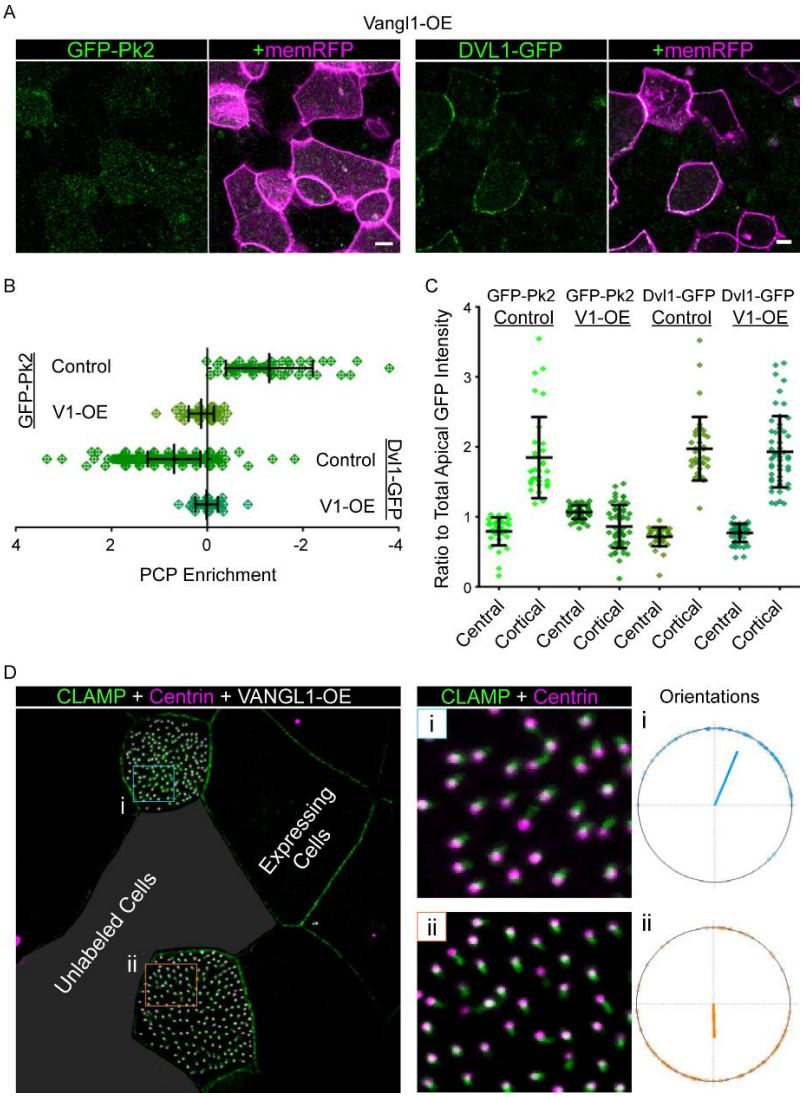

Fig. S4. Vangl1 Overexpression leads to PCP patterning and nonautonomous tissue-level polarity defects. (A) Cells in stage 31 embryos labeled with PCP proteins fused to GFP and membraneRFP as well as overexpressing Vangl1 display loss of Dvl1-GFP asymmetry and reduction in GFP-Pk2 cortical enrichment. Scale bars represent 10μm. (B) Graph depicting changes in PCP Enrichment of Pk2 and Dvl1 caused by Vangl1 overexpression (V1-OE). PCP enrichment is significantly reduced in cells overexpressing Vangl1 (n= 60 for Pk2, n= 55 for Dvl1) in comparison to controls for both GFP-Pk2 (n= 64) ($p<0.0001$***) and Dvl1-GFP (n=243) ($p<0.0001$***). Error bars indicate standard deviation of the mean. (C) Quantification data showing a significant loss of cortical enrichment of GFP-Pk2 but not Dvl1-GFP upon Vangl1 overexpression (V1-OE). Each dot represents one cell, and each cell has both a Central and a Cortical measurement presented as divided by the total apical fluorescence (See Fig. S3A for quantification schematic). These Central and Cortical measurements are highly significant from one another in both Pk (n= 33) and Dvl1 (n=6) control ($p<0.0001$***), Dvl1 with V1-OE (n= 53, $p<0.0001$***), and Pk2 with V1-OE (n= 53, $p=0.0002$***) conditions, but only in the case of GFP-Pk2 in V1-OE embryos is the mean Cortical enrichment less than the Central measure. Error bars indicate standard deviation of the mean. (D) Two multicilated cells situated at the edge of a clone labeled with Centrin-RFP and CLAMP-GFP and overexpressing Vangl1, with cell (i) outlined in blue situated above unlabeled cells and cell (ii) outlined in orange situated below. Magnification of boxed areas and quantification of ciliary orientations and mean polarity vector for each cell demonstrate the tendency for striated rootlets (opposite the effective stroke) to be oriented towards higher Vangl1 levels (towards labeled cells and away from unlabeled cells) (n= 95 orientations for i, n= 124 orientations in ii).

Development • Supplementary information

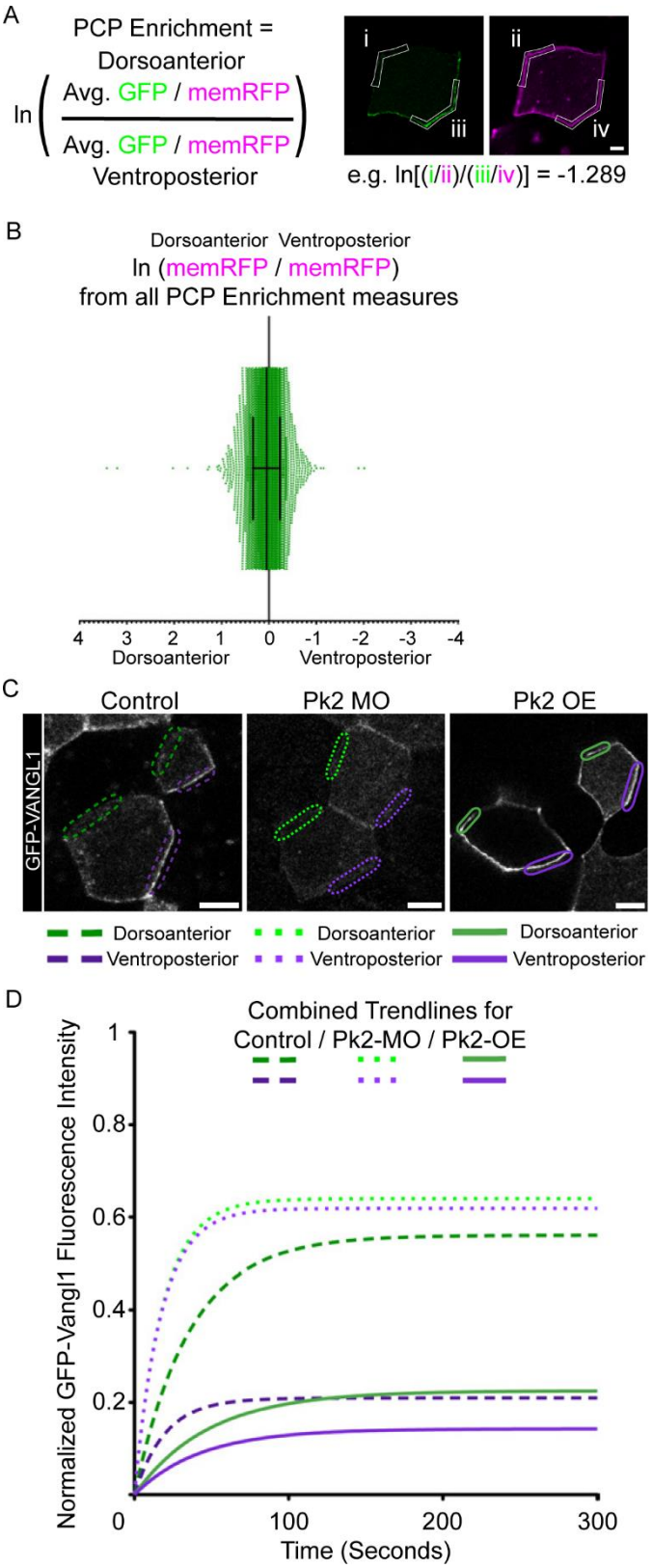

Fig. S5. Supplement for measures and quantifications. (A) Equation used and an example for calculating PCP Enrichment (GFP-Pk2 and memRFP shown). (B) Plot of enrichment values for dorsoanterior and the complementary ventroposterior membraneRFP measurements in consideration

Development • Supplementary information

without the associated GFP PCP fusion measurements for all PCP Enrichment measurements in presented in Fig.s 1-5. A value of 0 represents no difference in intensity. n=5,394. Error bars indicate standard deviation of the mean. (C) Demonstrations of typical shape and orientation of regions bleached and measured for intensity recovery quantifications shown in Fig. 4E and key for (D) below. Scale bar represents 10 μm. (D) Combined trendlines for data presented in Fig. 4E for a more direct comparison of recovery trends.

Development • Supplementary information

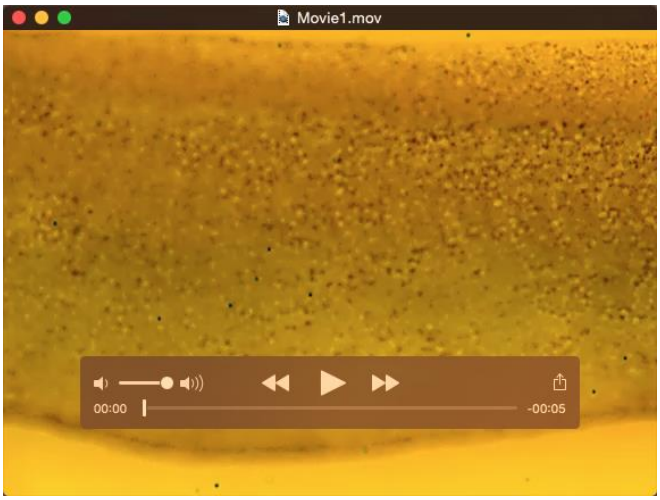

Supplementary Movie 1

Time-lapse movie of latex beads flowing across the epidermis of a control, uninjected stage 31 *Xenopus laevis* embryo.

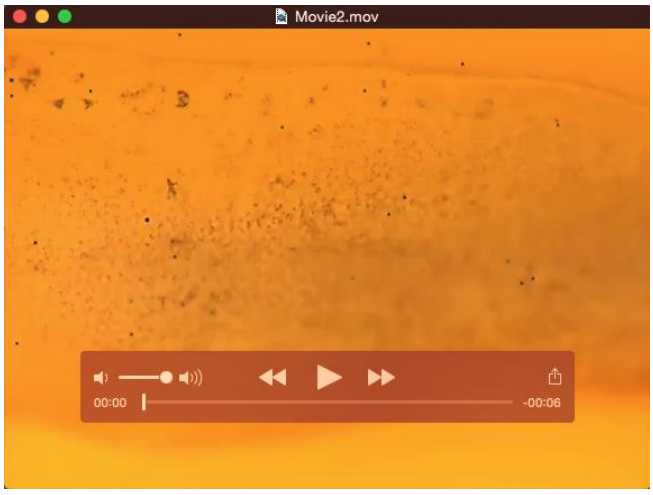

Supplementary Movie 2

Time-lapse movie of latex beads flowing across the epidermis of a stage 31 *Xenopus laevis* embryo injected with Pk2 morpholino (#1).

Development • Supplementary information

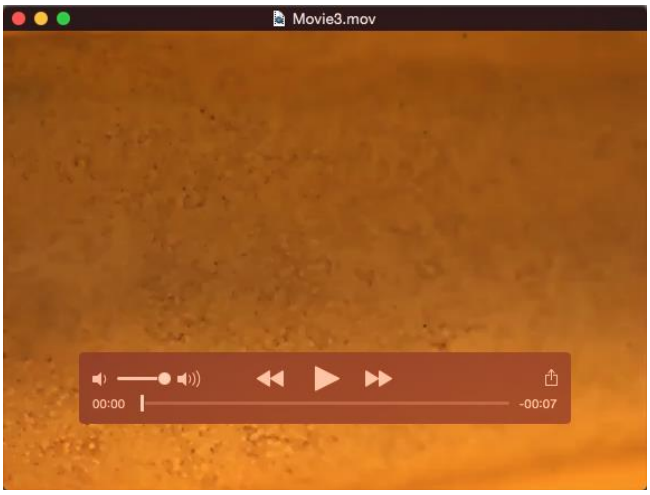

Supplementary Movie 3

Time-lapse movie of latex beads flowing across the epidermis of a stage 31 *Xenopus laevis* embryo overexpressing Vangl1.

Development • Supplementary information

Table S1. Primers (5′-3′)

Pk2 CS107-GFP

ATAGGCCTATGTTTAACCGGAGCTCTTGGACAAGGGCTTC and

ATGCGGCCGCCTAGGAGATGATGCAATTTTTGCTTTTTCGCCTTT

Pk2 for RFP-Pk2

CACCATGTTTAACCGGAGCTCTTGGACAAGGGCTTCCAGC and

CTAGGAGATGATGCAATTTTTGCTTTTTCGCCTTTTTCTG

Dvl1 (GenBank BC074103.1)

CACCATGGCTGAGACCAAAATCATCTACCATATAGATGAA and

CATGATGTCAACAAAGAATTCACAAGGGTTCCCCA

Dvl3 (NCBI ref NM_001092629.1)

CACCATGGGGGAGACCAAGGTCATCTACCACCTGGATGAA and

AACACCCCAGAATTCTTTGATAACATCCACAAAGAACTCA

Fzd6 (JGIv7b.000063404_134470-165935+)

CACCATGGATCTGATTGGCTGCTGCCTCCAAGCTCCGAGC and

CGCACTTGTCGTATTAATATTAATGTCATTGGCATGG

Vangl1 (JGIv7b.000169011_589431-599179+)

CACCATGGACACGGAATCCAACCACTCGGGATATTCACAT and

TCACAGGTTGGTCTCAGGTTTGCTACTCACAATGAGACGA

ΔPET-1

AGATGGCACCAGTCATGGTTACTGGGAAAAAGTCAAACATCAGCTTGTTC

ΔPET-2

AACTATGAACAAGCTGATGTTTGACTTTTTCCCAGTAACCATGACTGGTG

ΔPETΔLIM-1

AGGCGGAATCTGAAGAGTCCGAGCCATTAAAGTCAAACATCAGCTTGTTC

ΔPETΔLIM-2

Development • Supplementary information

AACTATGAACAAGCTGATGTTTGACTTTAATGGCTCGGACTCTTCAGATT

ΔC2-1

CCGTGATAATGAGCAACACTATCGACATTCTTCAGAGTCTGACAATGAAG

ΔC2-2

AGTATCCTTCATTGTCAGACTCTGAAGAATGTCGATAGTGTTGCTCATTA

Dvl1-ΔPDZ$_{partial}$

TGTAGCAGCGGATGGGCGTATTGAACCTATGGGCCCCTCCATGAGCATCATCACAT and

ATGTGATGATGCTCATGGAGGGGCCCATAGGTTCAATACGCCCATCCGCTGCTACA

Development • Supplementary information